Use of A-train satellite observations (CALIPSO-PARASOL) to evaluate tropical cloud properties in the LMDZ5 GCM

D. Konsta, J.-L D Dufresne, H Chepfer, A Idelkadi, G Cesana

Use of A-train satellite observations (CALIPSO-PARASOL) to evaluate tropical cloud properties in the LMDZ5 GCM

D. Konsta, J.-L. Dufresne, H. Chepfer, A. Idelkadi, G.Cesana

Laboratoire de Météorologie Dynamique (LMD/IPSL), Paris, France

LMD/IPSL, UMR 8539, CNRS, Ecole Normale Supérieure, Université Pierre et Marie Curie, Ecole Polytechnique

Abstract

The evaluation of key cloud properties such as cloud cover, vertical profile and optical depth as well as the analysis of their intercorrelation lead to greater confidence in climate change projections. In addition, the use of collocated and instantaneous data facilitates the links between observations and parameterizations of clouds in climate models.

New space-borne multi-instruments observations collected with the A-train make simultaneous and independent observations of the cloud cover and its three-dimensional structure at high spatial and temporal resolutions possible. The CALIPSO cloud cover and vertical structure and the PARASOL visible directional reflectance, which is a surrogate for the cloud optical depth, are used to evaluate the representation of cloudiness in two versions of the atmospheric component of the IPSL-CM5 climate model, LMDZ5 GCM. A model to satellite approach in applying the CFMIP Observation Simulation Package (COSP) is used to allow a quantitative comparison between model results and observations.

The representation of clouds in the two model versions is first evaluated using monthly mean data. This classical approach reveals model biases of different magnitudes depending on the model version used. These biases are an underestimation of cloud cover associated to an overestimation of cloud optical depth, an underestimation of low- and mid-level tropical clouds and an overestimation of high clouds. The difference between models of these biases clearly highlights the improvement of the amount of boundary layer clouds, the improvement of the properties of high-level clouds and the improvement in simulating mid-level clouds in the tropics thanks to the new convective, boundary layer, and cloud parameterizations included in LMDZ5B compared to the previous LMDZ5A version. The correlation between instantaneous cloud properties allows for a process-oriented evaluation for tropical oceanic clouds. This evaluation shows that the cloud population with intermediate values of cloud cover and cloud reflectance when using monthly mean is now split in two groups of clouds, one with low and intermediate values of the cloud cover and another one with cloud cover close to one. The precise determination of cloud height allows us to focus on specific types of clouds (i.e. boundary layer clouds, high clouds, low-level clouds with no clouds above). For low-level clouds over the tropical oceans, the correlation between instantaneous values of the cloud cover and cloud reflectance reveals a major bias in the simulated liquid water content for both model versions. The origin of this problem is determined and possible improvements such as considering the sub-grid heterogeneity of cloud properties are investigated using sensitivity tests. In summary, the analysis of the relationship between different instantaneous and collocated variables allows for process-oriented evaluations. These in turn may help to improve model parameterizations and may also help to bridge the gap between model evaluation and model development.

1. Introduction

The evaluation of clouds simulated by general circulation models (GCMs) generally relies on monthly mean values [e.g. Yu et al., 1996, Webb et al. 2001, Zhang et al. 2005], which do not contain detailed information on the transient aspects of cloud behavior. Using monthly mean values might lead to a quantitative way to calibrate models in order to match present-day observations with present-day simulations but these monthly means lack details on the cloud processes that create them.

The A-train jointly observes the cloud radiative properties using the passive remote sensors PARASOL (Polarization & Anisotropy of Reflectances for Atmospheric Sciences coupled with Observations from a Lidar) [e.g. Parol et al. , 2004] and CERES (Clouds and the Earth's Radiant Energy System) [Wielicki et al., 1996] as well as the cloud vertical structure using the new generation of satellites carrying lidar instruments CALIOP/CALIPSO (Cloud-Aerosol Lidar and Infra-red Pathfinder Satellite Observations) [Winker et al. 2007]. This joint observation dataset constitutes a unique opportunity to perform quantitative evaluations of GCM cloudiness [Chepfer et al., 2008, Marchand et al., 2009, Zhang et al., 2010, Cesana and Chepfer, 2013]. The ability of the A-train to simultaneously observe the radiative properties of clouds and their three-dimensional distribution at the instantaneous time scale (typically on the order of tens of seconds) and at high spatial resolution [Konsta et al., 2012] is used to provide new observational constraints to evaluate the representation of cloud processes in climate models.

A major aim of physical parameterizations in GCMs is to reproduce the mean properties of cloud variables as well as the relationships between these cloud variables and the dynamic and thermodynamic state of the atmosphere. If models fail to reproduce these key features, they may lack the ability to properly predict cloud variations under environmental changes, cloud feedbacks and the cloud response to anthropogenic forcing. A key step is thus to evaluate the mean properties of clouds and to evaluate how they vary in response to a change of the physical characteristics of their environment. The instantaneous analysis of cloud properties facilitates a direct relationship between observations and model parameterizations. Some meteorological features occur at instantaneous time scale but are lacking when using monthly mean values, such as the complex multi-layer structure of mesoscale convective systems or the inhomogeneous spatial structure of marine stratocumulus. These features have an important impact on the radiative effect of clouds and therefore on the magnitude of cloud feedbacks as the two are strongly correlated [Brient and Bony, 2012].

Short time scales may be considered during the development stage of a model. For instance, some recent developments in the LMDZ atmospheric model have been undertaken in order to improve the diurnal cycle of precipitation and to solve the long-standing problem of too early precipitations in tropical regions [Rio et al., 2013]. The following questions are addressed:

1) Have the recent developments in the LMDZ5B atmospheric model improved the representation of clouds' physical properties?

2) Can the instantaneous spatial observations allow for the identification of remaining problems in the model representation of clouds? and

3) What role plays the cloud heterogeneities at the model's subgrid scale for the remaining problems in representing cloud in models?

The simulated cloud occurrence, vertical structure and optical depth of tropical oceanic clouds are compared with A-train observations. Monthly mean values are first considered as it is the common time scale used in climate model evaluation. Instantaneous values are then used to facilitate the interpretation of results in term of model parameterization because the statistical relationships between cloud variables at these two time scales have been shown to be significantly different [Konsta et al., 2012]. Observations provided by CERES are used to evaluate the cloud shortwave radiative albedo, observations provided by PARASOL are used to evaluate the cloud optical depth, and observations provided by CALIOP/CALIPSO are used to evaluate the cloud cover and the cloud vertical profile.

The two versions of the LMDZ5 atmospheric model, the A-train observations and the observations simulators are briefly described in Section 2. The cloud properties simulated by the model are first evaluated using monthly mean observations of top-of-the-atmosphere fluxes, reflectance, cloud cover, and vertical structure (Section 3). A more advanced process-oriented evaluation is then conducted for tropical oceanic clouds based on the correlation between instantaneous cloud properties observed with the A-train. Illustrations of how this may help to improve model parameterizations are presented in Section 4. Conclusions are given in Section 5.

2. Methodology

2.1 The LMDZ5 climate model

LMDZ5 is the atmospheric component of the IPSL-CM5 climate model [Dufresne et al., 2013]. Two versions of this atmospheric model (LMDZ5A [Hourdin et al., 2013-a] and LMDZ5B [Hourdin et al., 2013-b]) are evaluated. Both model versions are described in cited papers and only key aspects are summarized here. LMDZ5A is similar to LMDZ4 [Hourdin et al., 2006] used in the previous version of the IPSL model [Marti et al., 2010] but it has an increased vertical resolution (from 19 to 39 vertical levels), an improved representation of the stratosphere and a modified horizontal grid (1.895° in latitude x 3.75° in longitude). LMDZ5B is a new model version that includes, in addition to LMDZ5A, many new developments on the physical parameterizations such as (i) a new scheme of the boundary layer, which combines a model of turbulent diffusion and a 'mass flux' scheme in order to represent the coherent structures of the dry or cloudy convective boundary layer [Rio and Hourdin, 2008, Rio et al., 2010] and a new low-level cloud scheme [Jam et al., 2011], (ii) a parameterization of the cold pools created by re-evaporation of convective rainfall [Grandpeix and Lafore, 2010], and (iii) a modification of the triggering and the closure of the Emanuel (1991) convective scheme based on the Available Lifting Energy for the triggering and Available Lifting Power for the closure [Rio et al., 2013]. All model results have been obtained with multi-years simulations over the period 1979-2009 in which the sea surface temperature and the sea-ice cover are prescribed to values close to observations (AMIP experiments).

2.2. Observations

Cloud cover and cloud vertical structure

Thanks to its vertically resolved measurements, to its high sensitivity to optically thin atmospheric layers and to its high horizontal resolution, the CALIOP/CALIPSO lidar [Winker et al. 2007] is well suited to accurately identify clear sky areas, aerosol regions [Liu et al. 2008, Vuolo et al. 2009], fractionated cloud covers such as the trade winds cumulus [Konsta et al., 2012, Medeiros et al., 2010], optically thin clouds such as the sub-visible cirrus clouds [Sassen et al. 2008, Noel et al. 2010, Martins et al. 2011], polar stratospheric clouds [Noel et al. 2008, Pitts et al. 2007, Noel et al. 2010], and to document the cloud vertical distribution of the atmosphere.

In order to compare the GCM results with CALIOP observations, a dedicated product called CALIPSO-GOCCP has been developed to be fully consistent with the lidar simulator [Chepfer et al. 2010]. This product consists in applying Scattering Ratio (SR) thresholds values to the 532nm lidar SR signal to detect the presence of clouds. The cloud detection (0 or 1) is done at the original horizontal Level 1 CALIOP resolution (330m along track and 75m cross-track of the satellite orbit) but on a lower vertical resolution (40 equidistant vertical levels of 480 m height). The cloud fraction is then built on a 2°x2° latitude/longitude grid to provide information on cloud cover, on low- mid- and high-levels cloud covers, and on vertical cloud distributions.

The monodirectional cloud reflectance: a surrogate for the cloud optical depth

The PARASOL instrument (POLDER-like, [Deschamps et al. 1994]) has a multi-viewing angle capability allowing for the estimation of the instantaneous monodirectional reflectance of clouds. The use of this level-1 product as a surrogate of the optical depth eliminates the need for many of the assumptions made during the retrieval process of the cloud optical thickness [Minnis et al., 1995]. The criteria used for the selection of the viewing angle are described below. Note that Cole et al. [2011] have computed and used CERES SW fluxes integrated over the diurnal cycle to perform a similar analysis but the PARASOL instantaneous monodirectional reflectance provides more precise information because it contains fewer assumptions than the CERES daily SW fluxes.

Above the ocean surface, the visible directional reflectance is defined as $\rho(\theta_s, \theta_v, \phi_s, \phi_v) = \pi\, L(\theta_s, \theta_v, \phi_s, \phi_v) / E_s\, \mu_s$, where θ_s, θ_v, ϕ_s, ϕ_v, are respectively the solar zenith angle, the zenithal viewing angle, the solar and viewing azimuth angles, L is the measured radiance, μ_s is the cosine of the solar zenith angle, and E_s the incident solar radiation. This directional reflectance is mostly sensitive to the solar zenith angle (θ_s), to the viewing direction (θ_v, ϕ_s-ϕ_v) and to the cloud optical depth. Some viewing directions are contaminated by the specular reflection of the solar light on the sea surface (i.e. sunglint), or are very dependent on cloud microphysical properties (e.g. particle shape through their optical properties). As the aim is to evaluate the optical depth, the reflectance observed in a single viewing direction that is mostly sensitive to the cloud optical depth and less to other parameters has been selected. The reflectance in a constant single direction has thus been selected all over the globe (Fig. A) in avoiding (i) directions with ($90° < \phi_s - \phi_v < 270°$) since they are sensitive to the glitter reflection, (ii) the backscattering direction, which is highly sensitive to the cloud microphysical properties, and (iii) the nadir direction, which is less sensitive to the optical depth than any other direction. Among the others possible directions, the one at 865nm, which is the more frequently observed by PARASOL all over the globe ($\theta_v = 27° \pm 2.5°$, $\phi_s - \phi_v = 320° \pm 2.5°$) was selected. All the directional reflectance values of spatial resolution of 6x6 km^2 measured by PARASOL in this direction are then projected onto a 2°x2° grid. The calibration of PARASOL is described by Fougnie et al. [2007]. The calibration accuracy is within 1.5% for the 865nm channel. The spatio-temporal sampling of PARASOL and CALIPSO observations is presented in Annex A.

Due to the difference of viewing angles and of pixel sizes between PARASOL and CALIPSO, cloudy and clear-sky properties cannot be separated at the pixel scale. The clear-sky and cloud properties are computed at the 2°x2° scale following the methodology proposed by [Konsta et al., 2012]. The monodirectional reflectance R averaged over each grid cell depends on the clear-sky reflectance (CSR), on the cloud cover (CC) and on the cloud reflectance (CR) in this grid cell according to the relation

$$R = CC \times CR + (1-CC) \times CSR. \qquad (2.1)$$

We assume that for each horizontal 2°x2° grid cell, the fraction CC of the highest values of monodirectional reflectance observed at the pixel level correspond to cloudy conditions and the fraction (1-CC) of the lowest values correspond to clear-sky conditions. In practice, the cloud cover CC is first determined from CALIPSO observations daily and for each 2°x2° grid cell. Then, the cloudy monodirectional reflectance CR is computed as the grid cell average of the fraction CC of the highest values of monodirectional reflectance observed by PARASOL at the pixel level. The clear-sky monodirectional reflectance CSR is the grid cell average of the fraction (1-CC) of the lowest values. Note that the cloud reflectance used here is different from the total reflectance generally used and which contains the contribution of clear-sky surrounding clouds. Except stated otherwise, the results and figures based on CALIPSO and PARASOL observations are for the two-year period 2007-2008.

2.3. PARASOL and CALIPSO simulators

By taking into account the effects of cloud overlap together with the specificities of the satellite, the model-to-satellite approach allows for a consistent comparison between the satellite observations described above (Section 2.2) and model outputs. The PARASOL and CALIPSO simulators have been designed for this purpose. The first step of the CALIPSO and PARASOL simulators consists in sub-gridding the model outputs (i.e. temperature, pressure, cloud cover, cloud condensate and effective radius of cloud droplets and ice crystals). The model vertical profiles are converted to an ensemble of subgrid-scale profiles by dividing each grid cell into a few tens of subcolumns generated randomly using the Subgrid Cloud Overlap Profile Sampler [Klein and Jakob 1999; Webb et al. 2001]. In each subcolumn, the cloud cover is assigned to be 0 or 1 at every model level with the constraint that the cloud condensate and cloud cover averaged over all subcolumns is consistent with the grid-averaged model diagnostics and the cloud overlap model assumption.

The monodirectional reflectance, the total cloud cover and the vertical cloud distribution as it would be seen by PARASOL and CALIPSO respectively are then computed in each subcolumn (see Chepfer et al. 2008 for CALIPSO and Annex B for PARASOL) and averaged over each model grid cell. Due to the large and highly variable reflection of solar light on ground surfaces, the PARASOL simulator is not used above continents.

Above oceanic regions, the cloud monodirectional reflectance CR is computed for every grid cell at each time step, using the same definition as for the observations (Eq. 2.1) :

$$CR = \frac{R - (1 - CC) \cdot CSR}{CC} \quad (2.2)$$

where the monodirectional reflectance R and the cloud cover CC have been previously computed by the simulator. The clear-sky reflectance has a fixed value in the simulator (CSR=0.03), which is consistent with the observations under clear-sky conditions [Konsta et al., 2012].

To simplify the post-processing of simulator outputs, the monodirectional reflectance is computed by the PARASOL simulator at every time step for a constant solar zenith angle corresponding to the A-train overpass at each latitude instead of the zenith angle corresponding to the local time in the GCM grid (Annex B). Sensitivity tests indicate that the cloud cover and reflectance computed by the PARASOL and CALIPSO simulator with the LMDZ model are almost insensitive to the frequency call of the simulator (every 1.5, 3, 6 hours), to the number of sub columns (if greater than 20 in each grid cell), and to the use of day or night time outputs (2% for the cloud cover and 2.5% for the reflectance; Figures not shown). In this study the simulator is called every 3 hours and 100 subcolumns are used.

As the reflectance is not commonly used for cloud description, an approximate relationship between cloud reflectance and cloud optical thickness is given. The cloud reflectance (CR) can be converted in cloud optical thickness ($C\tau$) using the coarse approximation of spherical particles when T>0^{o}C, non-spherical particles when T< 0^{o}C and θ_s=30° (see Annex B, Figure B.b). However, this cloud optical thickness should not be considered as the real cloud optical thickness but only as an approximation given for convenience. The rigorous comparison between models and observations should be made using the monodirectional reflectance. The same assumption to convert PARASOL cloud reflectances into cloud optical thicknesses are made for both observed and simulated data in order to make sure that this conversion does not introduce an artifact when comparing models and observations.

PARASOL and CALIPSO simulators are included in COSP (CFMIP Observational Simulator Package) [Bodas-Salcedo et al. 2011], which also includes other simulators such as the ISCCP [Klein and Jakob 1999; Webb et al. 2001] and the CloudSat [Haynes et al. 2007] simulators. The COSP simulator is available to the community via the Cloud Feedback Model Intercomparison Project (CFMIP) web page (cfmip.net) and the monthly and instantaneous datasets used here,, which are consistent with the COSP outputs, are available via the “CFMIP Observations for Model evaluation” website (climserv.ipsl.polytechnique.fr/cfmip-obs.html).

3. Assessment of cloud properties using monthly mean statistics

The basic properties of clouds simulated by climate models are usually evaluated by comparing monthly mean values of the observed TOA fluxes, cloud cover, cloud optical depth and cloud top height (ie. Zhang et al. 2005, Klein et al. 2013). In this section, this approach based on monthly mean statistics is followed to evaluate the two versions of the LMDZ climate model.

a) Cloud geographical distribution

An aim of the improvements in the LMDZ5B model compared to LMDZ5A was to improve the cloud cover [Hourdin et al., 2013-b] and this has been achieved in many regions. The cloud cover (CC) simulated by LMDZ5B is in better agreement with observations than the CC simulated by LMDZ5A over the North Pacific and the North Atlantic, over the warm pool (where there are high convective clouds), along the East coast of the oceans and over the trade wind regions (where cumulus clouds dominate) but the CC values are still too low (Annex C). When considering the zonal mean values, LMDZ5B still underestimates the cloud cover in the tropics even though the bias is reduced by a factor of two compared to LMDZ5A.

High-level clouds feature a better vertical distribution in LMDZ5B than in LMDZ5A with a lower cloud cover but this CC is still too high (Annex C). LMDZ5B is able to simulate mid-level clouds even though they are still too few. Low-level clouds are also better simulated in LMDZ5B with a larger cloud cover but the low-level clouds are too low and they are too concentrated in one single layer. At middle and high latitudes, LMDZ5B simulates relatively well the large vertical extent of the frontal clouds associated with storms. The cloud fraction is improved in LMDZ5B compared to LMDZ5A but the cloud reflectance is not. Cloud reflectance and therefore cloud optical thickness are strongly overestimated by both model versions almost everywhere and in particular over the subtropical oceans and in mid and high latitudes (Annex C).

b) Tropical oceanic clouds in dynamical regimes

Based on their geographical distribution the cloud properties discussed in the previous sections can be summarized in the tropics using dynamical regimes [Bony et al., 2004]. Figure 1 shows the monthly mean cloud cover (Fig. 1a), cloud reflectance (Fig. 1b) and SW albedo (Fig. 1c) as a function of the monthly mean vertical velocity at 500hPa (ω_{500}), as well as the PDF of ω_{500} (Fig. 1d) over the tropical ocean. In the convective regions (ω_{500}<0), the cloud cover simulated by LMDZ5B is closer to observations than the cloud cover simulated by LMDZ5A whereas in subsidence regions where ω_{500}>20 hPa/day, the cloud cover is underestimated in both model versions (Fig. 1a). The cloud reflectance is strongly overestimated in both model versions, this overestimation being smaller in convective regions where ω_{500}<-40 hPa/day (Fig, 1b). Despite these large discrepancies, both model versions simulate reasonably well the SW albedo in subsidence regions (ω_{500}>0, Fig. 1c), which dominates in the Tropics (65% of the surface of the entire tropical belt). Even though both model versions reproduce well the mean value and the overall geographical pattern of the albedo (Figures not shown), they do not succeed in simulating properly the cloud cover and the cloud reflectance.

c) Correlation between cloud top pressure and cloud optical thickness over the tropical ocean

The joint histograms of cloud top pressure (CTP) and cloud optical thickness (Cτ) obtained with ISCCP data [Rossow and Schiffer, 1991] have been widely used for atmospheric studies [e.g. Jakob and Tselioudis 2003, Rossow et al. 2005] and for model evaluation [e.g. Webb et al, 2001, Williams and Tselioudis, 2007, Klein et al., 2013]. They are computed using two methods. In the first method, the ISCCP-D2 data and ISCCP simulator outputs are directly used (Fig. 2d-f). In the second method, the CALIPSO and PARASOL data and simulator outputs are used and CTP is defined as the pressure of the highest level where the instantaneous CALIPSO-GOCCP cloud cover in each 2°x2° grid cell is greater than 0.1 (Fig. 2a-c). Sensitivity tests show that results are not very sensitive to the value of this threshold when it varies from 0.1 to 0.3. The cloud optical thickness Cτ is computed from the cloud reflectance. The 2D histogram features these instantaneous CTP and Cτ data for each grid cell and averaged over time.

The histogram based on ISCCP data (Fig. 2d) is very different from the one based on CALIPSO-PARASOL data (Fig. 2a). The 2D histogram over the tropical ocean obtained with the observed CALIPSO-GOCCP and PARASOL data (Fig. 2a) features two distinct populations, the first one in the high troposphere and the second one in the low troposphere. The histogram based on ISCCP data features a single cluster in the middle of the troposphere. This difference is a direct consequence of the much-improved measurement of cloud height by active sensors (CALIPSO) compared to passive ones (ISCCP), as already shown by Chepfer et al. [2008]. A more advanced comparison between ISSCP and merged CloudSat and CALIPSO histograms is described in Mace and Wrenn [2013].

Similar features are also visible in the model results where two populations of low and high clouds are featured when using the CALIPSO and PARASOL simulators (Fig. 2.b-c) and one single cluster of high clouds is featured when using the ISCCP simulator (Fig. 2.e-f). The main biases of the models (e.g. too many high clouds, too few low clouds, too high cloud optical thickness) also appear when using ISCCP observed and simulated data. However low clouds can be evaluated using CALIPSO but they do not occur when the ISCCP simulator is applied. Similarly, the optically thin clouds can be evaluated using CALIPSO but they are not detected in ISCCP observations nor simulated by the ISCCP simulator.

4. An advanced "process oriented" evaluation of tropical clouds description taking full advantage of the A-train capability

4.1 The added value of evaluating the model using instantaneous cloud properties

For climate change and climate variability studies, it is important to characterize and assess how cloud properties vary as a function of atmospheric variables describing the clouds environment. For example in climate feedbacks studies, changes ΔE of the cloud environment variables are assumed to depend on the change ΔT of the surface temperature (e.g. Colman and McAvaney, 1997, Soden and Held, 2006, Bony et al., 2006) and cloud properties are therefore assumed to vary as a function of the surface temperature. Within this framework, various studies (e.g. Bony et al., 2004, Webb et al., 2006) have analyzed how the cloud radiative effects vary in response to a change of the surface temperature at inter-annual time scales or under climate change situations. This approach has been successful to improve our understanding of cloud feedbacks but the temporal scale used in those studies (in general monthly mean variables) does not allow for the understanding of the direct relationship between these results and the model parameterizations. Indeed, cloud properties vary instantaneously in parameterizations (or with small time constants) when variables describing the environment (e.g. atmospheric stability, humidity) vary. These dependencies between cloud and environment characteristics are highly non-linear so that the relationship between these instantaneous variables may be very different from the relationship between their monthly or seasonal mean values. The A-Train offers new possibilities to analyze the correlation between instantaneous cloud cover and cloud reflectance in more detail.

Assuming for simplicity reasons that the clear-sky reflectance over ocean is negligible, the variation ΔR of the reflectance R (eq. 2.1.) depends on how the cloud cover (CC) and the cloud reflectance (CR) vary:

$$\Delta R \approx CR.\Delta CC + CC.\Delta CR.$$

The variation ΔR will be very different if the variations ΔCC and ΔCR have the same or the opposite sign. The CC and the CR variables estimated at the same time and location, as well as their joint variations are analyzed with a focus on the case where they vary in the same or opposite way. An evaluation of how cloud properties vary with the environment is more constraining for the models than an evaluation of the mean state and this may be one way to increase the confidence in model results.

The relationship between cloud cover and optical thickness over the tropical oceans is shown in Figure 3. In observations, this relationship has been shown to be significantly different when using monthly or instantaneous values [Konsta et al., 2012]. When using monthly mean data (Fig. 3, lower line), the observations show an almost linear relationship between the two variables: as the cloud cover increases, the cloud optical depth increases too (Fig. 3-d). The two versions of the model show very different behaviors from what is observed: the cloud optical depth remains almost constant when the cloud cover varies. LMDZ5A does not simulate the highest values of cloud cover and the simulated cloud reflectance is too high on average (Fig. 3-e). LMDZ5B simulates clouds that have a large cover and a reflectance consistent with observations, but clouds with a small cover have a too large reflectance (Fig. 3-f).

The use of instantaneous data gives a more accurate picture of the relationship between cloud cover and cloud optical depth and, for the models, a very different picture from what is observed (Fig. 3, upper line). For the observations, there is a tendency of increasing cloud reflectance with increasing cloud cover as it is the case for monthly mean values. But the instantaneous data reveal two separate cloud populations: one with a low cloud cover (CC<60%) and a low reflectance (CR<0.2) and another one with a cloud cover close to 1 and a cloud reflectance value ranging from 0.1 up to 0.9 (Fig. 3-a). Intermediate cloud reflectance (0.2-0.4) and cloud cover (0.5-0.8) values occur when using monthly mean values but are much less frequent when using instantaneous values. These intermediate values therefore do not correspond to actual clouds. Both model versions simulate clouds with a low cover but their reflectances are much too high (Fig. 3-b,c). LMDZ5A simulates few clouds with a cover close to one whereas LMDZ5B simulates many clouds with a cover close to one, as observed. However, the cloud reflectance-cloud cover relationship for both model versions does not show an increase of the cloud reflectance with cloud cover, as this is the case in the observations. The LMDZ5B model even shows an opposite relationship.

The instantaneous correlation between cloud variables constitutes a key test to improve the confidence in how cloud properties simulated by climate models vary in changing situations. Fig. 3 clearly shows that this test is highly challenging. Instantaneous cloud properties are analyzed below.

4.2. Evaluation of tropical clouds using instantaneous clouds properties

4.2.a Optical thickness of clouds and their vertical distribution

The PDF of the cloud reflectance (CR) observed by PARASOL, and simulated by the model and by the PARASOL simulator (Figure 4a), confirms that both model versions strongly overestimate the cloud reflectance. The cloud population is divided into three different classes according to their optical thickness: (i) the optically thin and intermediate clouds (CR<0.2, i.e. $C\tau$<3,41) corresponding to 55%, 29% and 25% of the clouds for the observations, the LMDZ5A and the LMDZ5B model respectively, (ii) optically thick clouds (0.2<CR<0.5, i.e 3.41<$C\tau$<11.42) corresponding to 34%, 50% and 53% of the clouds for the observations, LMDZ5A and LMDZ5B respectively, and (iii) very thick clouds (CR>0.5, i.e.

$C\tau>11.42$) corresponding to the less populated class: 11%, 21% and 22% for the observations, LMDZ5A and LMDZ5B respectively. The mean vertical profile of the cloud fraction observed from CALIPSO-GOCCP and simulated by the model and by the simulator is shown on Fig.4b-d for the three cloud classes. Note that the cloud reflectance is a vertically integrated value and characterizes the whole atmospheric column, while the cloud fraction is a local value at each vertical level. For optically thin and intermediate clouds (i.e. when $C\tau<3$ or $CR<0.2$) the lidar traverses clouds and provides information for the whole atmosphere whereas for thicker clouds ($CR>0.2$) the lidar signal is attenuated and does not provide information below the higher thick clouds.

Observations show that optically thin and intermediate clouds ($CR<0.2$, i.e. $C\tau<3.4$, Fig.4b) are mainly low-level clouds with low values of cloud fraction ($CF\approx0.15$). For the same range of optical thickness, both versions of the model simulate high-level clouds with intermediate values of the cloud fraction ($CF\approx0.27$). LMDZ5A does not simulate any low-level clouds while LMDZ5B simulates some but too few of them ($CF<0.05$). For optically thick clouds ($0.2<CR<0.5$, Fig.4c), both model versions correctly simulate high-level clouds with a mean cloud fraction ($CF\approx0.17$) and altitude close to the observations. Both model versions simulate low clouds with a correct fraction but a too low altitude, and they fail to simulate mid-level clouds. Lastly, optically very thick clouds ($CR>0.5$, Fig.4d) are mainly high-level clouds with a large cloud fraction ($CF\approx0.37$) with some mid-level clouds ($CF\approx0.2$) and only a few low-level clouds. The two model versions simulate optically very thick clouds with a very different cloud vertical structure, with much less high-level clouds ($CF\approx0.15$ for LMDZ5A and 0.06 for LMDZ5B), almost no mid-level clouds and a fraction of low-level clouds ($CF\approx0.1$) close to observations, also smaller.

In summary, the fraction of mid- and high-levels clouds increases with the cloud reflectance in the observations but decreases in the models. The fraction of low-level clouds in the observation and in the models does not show a tendency of change with cloud reflectance, and the altitude of the simulated clouds is generally too low.

4.2.b. Focus on high-level clouds

In ascent regions, 2°x2° grid cells with no high-level clouds ($P<440$ hPa) are rarely observed (15% of the time, Fig. 5-a) and rarely simulated by both models (10 to 20% of the time). The cumulative distribution function (CDF) of high-level cloud cover regularly increases (their frequency of occurrence is almost constant) until it becomes close to one. For these very cloudy conditions, there is a rapid increase in the CDF. The frequency of occurrence is much larger (typically 5 to 10 times) when the cloud cover is close to 1 than when it is smaller. The cloud cover of high-level clouds is larger than 95% in more than 25% of the situations. LMDZ5A simulates too few of these high-level clouds with a large cover but simulates too many high-level clouds with a too low cover compared to observations. On the contrary, LMDZ5B simulates too many high clouds with a large cover and the high-cloud cover is larger than 95% in 40% of the situations. Situations with almost no high-level clouds are much more frequent in subsidence regions (≈40% of the cases, Fig. 5-b) than in ascent regions and situations with a large cover of high-level clouds are rare. Both model versions simulate the observed general behaviors of clouds although LMDZ5B is closer to observations. The normalized cloud cover of high-level cloud is now used to show how the different height categories (here, high clouds) are divided among all observed clouds [Stubenrauch et al., 2012]. The normalized cloud cover of high-level cloud is defined as NCC_high = CC_high/CC, where CC_high is the cloud cover of high-level clouds and CC is the total cloud cover [Konsta et al., 2012]. In ascent regions, the observed normalized high-cloud cover regularly increases with the total cloud cover (except for very small cloud cover) and reaches values close to one in fully overcast situations (Fig. 5-c). When the total cloud cover is small the high-level clouds have a small contribution to the total cloud cover, which means that mid- and low-level clouds dominate. On the contrary, high-level clouds dominate when the cloud cover is close to one. In LMDZ5A, high-level clouds always dominate even when the total cloud cover is small. This model fails to simulate enough mid- and low-level clouds in ascent regions. This bias is also in LMDZ5B but to a much lesser extent. In subsidence regions, the observed normalized high cloud cover is small and increases with the cloud cover (Fig. 5-d). Low-level clouds dominate, as expected. Both model versions simulate a too large normalized cover of high clouds, which is consistent with a too small value of the low-level cloud cover in these regions.

4.2.c. Focus on boundary layer clouds

Low-level clouds over the tropical oceans are now examined. To do so, only the atmospheric columns where low-level clouds are dominant are considered. These columns are defined as the 2°x2° grid cells where the normalized cover of low-level clouds (P>680 hPa) is greater than 90% (CC_low/CC>90%). Figure 6 presents the relationship between the cloud cover and the cloud reflectance in these situations. The observed clouds may be organized in two groups (Fig. 6-a). In the first group, clouds have a small cover and a small reflectance. Further analysis shows that these clouds are present all over the tropics, with the most dominant population confined in the trade cumulus regions. Their properties are consistent with those of small cumulus clouds. The second group is composed of clouds with cover close to one and with a large reflectance (0.3<CR<0.6), i.e. a large optical thickness (5.5< Cτ<17). They are mainly located on the east coast of the tropical oceans and their properties are consistent with those of stratocumulus clouds. The results shown in Fig 6-a are broadly consistent with those obtained by Cole et al. [2011] using CERES and MODIS observations (their Fig. 7). The LMDZ5A model results show very different characteristics (Fig. 6-b) with most of the low-level clouds having a too large cloud cover and a too large reflectance, i.e. a too large optical thickness. The LMDZ5B model simulates two clusters of low-level clouds, one with small cloud cover values and another one with a cloud cover close to one, which is more consistent with observations.

However, when the cloud cover is small, the reflectance is much too large and increases when the cloud cover decreases, unlike in the observations.

This relationship is further examined by focusing on specific cloud regimes, following the methodology proposed by Medeiros and Stevens [2011] that allows for a separation in stratocumulus and shallow cumulus regimes. The stratocumulus regime corresponds to a regime where clouds have the largest values of cloud cover and cloud reflectance both in the observations and in the model. The shallow cumulus regime corresponds to clouds with smallest values of cloud cover and cloud reflectance (Figures not shown). For the stratocumulus regime, the observed relationship between cloud cover and cloud reflectance is quasi linear. The same relationship is also examined using the ISCCP 3hourly observations on the 2°x2° grid and the ISCCP simulator (Fig. 6d,e,f). The ISCCP cloud optical thickness is converted into cloud reflectance by assuming a fixed solar zenith angle θ_s=30° and spherical particles. The results from ISCCP are consistent with those obtained with CALIPSO-PARASOL, both for the observations and the models. However, the confidence in CALIPSO-PARASOL data is higher because the detection of low-level clouds is much better compared to ISCCP, as noted above. In CALIPSO-PARASOL data, cumulus clouds are found to have larger values of cloud cover compared to ISCCP observations. The decrease of cloud reflectance with cloud cover observed with CALIPSO-PARASOL is not evident with ISCCP.

According to theory and observation, the cloud optical thickness increases with the cloud top height for low-level clouds of same base height: as the cloud grows vertically, there is more water to condensate and the cloud optical depth increases. This relationship is a function of many phenomena (e.g. turbulent mixing, precipitation efficiency) that are not accurately known. This motivated many field campaigns [e.g. Coakley et al., 2005, Siebesma et al., 2003]. The analysis of this relationship on the global scale is performed using the CALIPSO-PARASOL observations. Figure 7 shows the mean cloud reflectance as a function of the cloud top pressure when low-level clouds are dominant. The cloud top pressure is defined as the first layer going downward from the 680hPa where the cloud cover is greater than 0.1. Both model and observations show that the cloud optical depth increases with cloud top altitude, as expected. However, the cloud optical thickness simulated by the models is two to three times larger than the observed one.

The poor representation of the low-cloud properties by the models may have important consequences for climate change studies. Indeed, low-level clouds cover most of the tropical ocean and are the main source of spread in climate sensitivity estimates [Bony and Dufresne, 2005; Vial et al., 2013]. In addition, the amplitude of the low-level cloud feedback depends on the cloud radiative effect [Brient and Bony, 2012] and an error in the later may impact the value of the former.

4.3. From model evaluation to model improvement

The analysis of monthly mean values confirm that the LMDZ5 model, as many other models, simulate low-level clouds with a too low cloud cover and a too high optical thickness (Nam et al. 2012, Klein et al. 2013). The use of instantaneous values further highlights the fact that the mean values as well as the variation of the cloud optical thickness with the cloud cover in the LMDZ model were biased. Key deficiencies in the model parameterizations can be identified and improved using the diagnostics presented above. Presenting new parameterizations for low-level clouds is far beyond the scope of this paper but the proposed diagnostics are very relevant for future model developments. The major discrepancy in models compared to observations identified above with increasing optical thickness as the cloud cover decreases, (Fig. 6) is further analyzed in the LMDZ5A model.

Many factors affect both the cloud cover and the cloud reflectance but a sensitivity analysis shows that the main driver of the erroneous relationship between these two variables in the LMDZ5A model is the liquid water content and not the micro-physic properties of clouds such as the cloud droplet size. The vertical integrated cloud water amount (or liquid water path) for low-level clouds increases as the cloud cover increases, like the cloud reflectance increases as the cloud cover increases, and the liquid water path is strongly correlated with the cloud reflectance (Figure 8-a).

The cloud fraction and liquid water content in the LMDZ5A model are diagnosed from the large-scale value of the total (vapor + condensed) water Q_t , the moisture at saturation Q_s , and the subgrid scale variability of the total water using a generalized log-normal Probability Distribution Function (PDF) defined by three statistical moments (mean, variance, skewness) (Bony and Emanuel, 2001 ; Hourdin et al., 2006). This parameterization was originally developed for convective clouds and then applied for all cloud types. Off-line calculations show that the increase of cloud reflectance when decreasing cloud cover (Fig. 6-b) cannot be explained under the conditions that generally exist when low-level clouds are present. This increase of cloud reflectance when the cloud fraction decreases is due to the deep convection scheme, which was activated quite frequently, without producing any deep convective clouds but affecting the PDF of the total water content at low level and therefore the cloud properties there. Sensitivity simulations confirm this hypothesis and show that the cluster of points in the upper left part of Fig. 6-b with high cloud reflectance and low cloud cover no longer exists when the deep convection scheme is switched off. However, the observed increase of reflectance with cloud cover is not reproduced by the model.

An implicit assumption of most (if not all) PDF parameterization approaches is that the sub-grid cloud cover is homogeneous (i.e. is either 0 or 1) in the vertical in each atmospheric layer. This assumption may be relevant when the sub-grid total water content is far above or far below the moisture at saturation but it may be questionable when the two values are similar. A very simple test is therefore performed to check the sensitivity of the cloud characteristics to this assumption. The equation for the liquid water content is assumed to be unchanged and clouds are assumed to only cover a vertical fraction of the atmospheric layer when the sub-grid humidity is close to the saturation and that this vertical fraction varies linearly from 0 when $Q_t = Q_s - \Delta Q$ to 1 when $Q_t = Q_s + \Delta Q$. In practical terms, the only change is to use $Q_s - \Delta Q$ instead of Q_s in the cloud cover formula. For the vertical spread of the humidity ΔQ, the same value as the one used to characterize the horizontal spread of humidity (Hourdin et al., 2006) is used. The typical values of $\Delta Q/Q_t$ are about a few percent and are comparable with the change of Qs due to the vertical gradient of temperature within an atmospheric layer. These values of the vertical spread of humidity are assumed to be realistic even though this choice is arbitrary and only relevant for a sensitivity test. The impact of this change on the cloud cover and on the relationship between cloud cover and cloud reflectance is very large for all clouds (Fig. 8-b to compare with Fig. 3 -b) and for conditions where low-level clouds are dominant (Fig. 8-c to compare with Fig. 6-b). Above all, the cloud reflectance increases with the cloud cover, which is consistent with observations and opposite to the results obtained with the original parameterization. A direct consequence is a modification of the SW flux at the TOA of about 10 W/m^{-2}. The geographical distribution of the simulated cloud reflectance is much closer to the observed values and the cloud cover is more realistic with more mid- and low-level clouds simulated, which is closer to the observed vertical structure of clouds. Although much more work is required to develop a new parameterization, the sensitivity test presented here illustrates the fact that the diagnostic is accurate enough to help identifying the origins of a major problem in the simulated low-level cloud properties and to show the direct effect of a specific modification of the model parameterizations.

Various studies have already analyzed how the effect of sub-grid heterogeneity of cloud properties may affect the parameterization of cloud radiative properties [e.g. Barker and Wielicki, 1997; Li et al. 2005] or autoconversion rate [e.g. Kawai and Texeira, 2012; Boutle et al., 2014], but very few have analyzed the effect of sub-grid heterogeneity of cloud properties on the parameterization of cloud cover even though this possibly large effect has been recognized [Pincus and Klein, 2000]. Based on results obtained with large eddy simulation (LES) models, Neggers et al. [2011] found that this effect is large for cumulus cloud type, which is consistent with the present hypothesis. To our knowledge few (if any) atmospheric models consider this phenomena in their parameterization. The possible role of this simplification on the tendency of models to simulate too few and too bright clouds deserve further investigation and is beyond the scope of this study.

5. Summary and conclusion

An evaluation of cloud characteristics (e.g. cloud cover, cloud vertical distribution and cloud optical depth) simulated by two versions of the LMDZ5 GCM using observations from PARASOL and CALIPSO has been presented. Model and observations have been compared using “observations simulators”, which allow direct comparisons between modeled and level 1 observed data by taking into account the spatial scale differences between model and observations and by avoiding most of the *apriori* hypothesis usually made in retrieval algorithms. This evaluation was performed using both monthly mean and instantaneous values and it has been shown how the latter allows for further analysis and may be used to help improve cloud parameterizations.

The comparison between the two versions of the LMDZ5 model and PARASOL/CALIPSO observations using the monthly mean climatologies clearly shows an improvement in the representation of cloud cover and cloud vertical distribution of LMDZ5B compared to LMDZ5A. This improvement consists of an increase of the cover of the boundary layer clouds especially in the trade wind regions, an improvement of the altitude and, to a less extent, of the fraction of the high-level clouds and the simulation of the large vertical extent of the frontal clouds associated with storms in the middle and high latitudes. Although reduced, some model biases in LMDZ5A are still present in LMDZ5B and are generally shared with many climate models, such as the lack of mid-level clouds in the mid latitudes [Chepfer et al., 2008, Zhang et al., 2005], the presence of optically too thick high-level clouds all around the globe [Zhang et al., 2005], and the lack of boundary layer clouds all around the tropical belt (in particular in the trade wind regions). Both versions of LMDZ5 model simulate the SW albedo well although they strongly overestimate the cloud optical depth. This suggests some compensating error between the cloud cover and the cloud optical depth and this compensation is different for the two model versions.

When using the instantaneous relationship between the cloud properties, new features appear and more precise conclusions may be drawn. Over the tropical oceanic regions, the following results are obtained:

1. Observed clouds are grouped in two clusters, one where clouds have a low to mid cover ($CC<60\%$) and a low reflectance ($CR<0.2$) and another one with a cover close to 1 and a reflectance that ranges from 0.1 to 0.9. The two model versions reproduce these two clusters but with a lack of fully overcast situations ($CC=1$) in LMDZ5A. In both model versions, there

are too few clouds with a small cover and their reflectance is strongly overestimated. There is a general tendency of increasing cloud reflectance with increasing cloud cover in observations and the models do not reproduce this tendency. Note that the relation between cloud fraction and cloud optical thickness are very different when using monthly mean or instantaneous values both in observations and in the models.

2. The CALIPSO-GOCCP data allow for a detailed description of the vertical distribution of clouds. In the observations, the fraction of mid- and high-levels clouds increases with the all clouds reflectance, whereas it decreases in the models. In ascent regions, there are frequent situations where grid cells are fully overcast with high-level clouds (CC_high>95%): 25% in observations, 10% and 40% in LMDZ5A and LMDZ5B respectively. In observations high-level clouds co-exist with low- and mid-level clouds whereas the multi-layer clouds are much less frequent in models.

3. The tropical low-level cloud properties can be grouped in two clusters. The first one corresponds to cumulus-type clouds and the second one corresponds to stratocumulus-type clouds. Observations show that the cloud optical depth increases with cloud cover and none of the model versions reproduce this general trend; they may even feature an opposite trend. Both models underestimate the low-level cloud cover but overestimate their reflectance. They do not produce enough low-level clouds and the low-level clouds they produce are too thick. These two biases partly compensate each other when considering the SW albedo. On average, the altitude of the low-level clouds simulated by the models is too low.

4. The relationship between instantaneous cloud cover and cloud reflectance for low-level clouds may be directly compared to what is expected from the parameterizations in these conditions. This diagnostic allows for the identification of key deficiencies in the parameterization and their origin as well as for possible improvements. More precisely, part of the problem is due to intermittent triggering of the convection and another part of the problem is due to a too large in-cloud liquid water amount. For the latter, the origin of the problem is believed to be the assumption of current parameterization that the cloud covers is homogeneous all along the vertical in each atmospheric layer. Sensitivity tests were performed and have shown that suppressing this assumption may have a large impact, leading to potential improvements in the cloud characteristics. More work is required to go from these sensitivity experiments to establishing useful new parameterizations.

Multi-instrument missions like the A-train offer the possibility to observe many properties of the clouds and their environment, which allows for a better evaluation of the climate simulated by atmospheric models. Beyond the separate analysis of each variable, the analysis of their joint variations allows for a deeper analysis and a better understanding of the dominant physical processes driving cloud properties. This is the case when using monthly mean values and using instantaneous data is even more powerful. Even if the instantaneous observations are less precise than averaged values and even if the collocation procedure may lead to the rejection of many observations, the analysis of their joint variations allows for a more precise evaluation of cloud properties, it may highlight new features or problems, it may facilitate the link between observations and parameterizations. It may also help to bridge the gap between model evaluation and model development.

Acknowledgments

The authors would like to thank CNES and NASA for the PARASOL and CALIPSO data, CGTD/ICARE for the collocation of the CALIOP L1 and PARASOL L1 datasets, Climserv/ICARE for the data access and for the computing resources. This research was partly supported by the FP7 European projects EUCLIPSE (# 244067) and IS-ENES2 (#312979). We also thank D. Tanré and F. Ducos for providing PARASOL monodirectional reflectance observations, Michel Viollier for fruitful discussions on CERES and PARASOL data, Michel Capderou for his useful comment on the A-train orbit, J. Riedi for its help to built Fig. 1A, and S. Bony for useful discussions. We strongly acknowledge the editor and the reviewers for their numerous suggestions that have helped us to improve the manuscript.

References

Barker HW, Wielicki BA., 1997. Parameterizing grid-averaged longwave fluxes for inhomogeneous marine boundary layer clouds. J. Atm. Sci. 54(24): 2785-2798.

Bodas-Salcedo A, M. J. Webb, S. Bony, H. Chepfer, J.-L. Dufresne, S. A. Klein, Y. Zhang, R. Marchand, J. M. Haynes, R. Pincus, V. O. John, 2011: COSP: satellite simulation software for model assessment. Bull. Amer. Met. Soc., 92(8), doi:10.1175/2011BAMS2856.1

Bony S., J.-L. Dufresne, H. Le Treut, J.-J. Morcette and C. Senior, 2004 : On dynamic and thermodynamic components of cloud changes. Clim. Dyn., 22, 71-86.

Bony S. and J.-L. Dufresne, 2005: Marine boundary layer clouds at the heart of tropical cloud feedback uncertainties in climate models, *Geophys. Res. Lett.*, 32, No. 20, L20806, doi:10.1029/2005GL023851.

Bony S., R. Colman, V. M. Kattsov, R. P. Allan, C. S. Bretherton, J.-L. Dufresne, A. Hall, S. Hallegatte, M.M. Holland, W. Ingram, D. A. Randall, B.J. Soden, G. Tselioudis and M. J. Webb, 2006: How well do we understand and evaluate climate change feedback processes? J. Climate, 19, 3445-3482.

Boutle IA, Abel SJ, Hill PG, Morcrette CJ., 2014. Spatial variability of liquid cloud and rain: observations and microphysical effects. Q. J. R. Meteorol. Soc. 140: 583-594. DOI:10.1002/qj.2140

Brient F. and S. Bony, 2012: How may the low-cloud radiative properties simulated in the current climate influence the low-cloud feedbacks under global warming? Geophys. Res. Lett., 39, L20807, doi:10.1029/2012GL053265.

Cesana G. and H. Chepfer, 2013: Evaluation of the cloud thermodynamic phase in a climate model using CALIPSO-GOCCP. Geophys. Res. Lett., 118,7922-7937, doi:10.1002/jgrd.50376.

Coakley J.A., M.A. Friedman and W.R. Tahnk, 2005: Retrievals of cloud properties for partly cloudy imager pixels. J. Atmos. Ocean. Tech. 22, 3-17.

Cole J., H. W. Barker, N. G. Loeb, K. von Salzen, 2011: Assessing Simulated Clouds and Radiative Fluxes Using Properties of Clouds Whose Tops are Exposed to Space. *J. Climate*, 24, 2715-2727, doi: 10.1175/2011JCLI3652.1

Colman R. and B. J. McAvaney, 1997: A study of general circulation model climate feedbacks determined from perturbed SST experiments. J. Geophys. Res., 102, 19 383–19 402.

Chepfer H., P. Minnis, D. Young, L. Nguyen, and R. F. Arduini, 2002: Retrieval of cirrus cloud ice crystal shapes using visible reflectances from dual-satellite measurements, *J. Geophys Res; 107*, 10.1029/2000JD000240.

Chepfer, H., S. Bony, D. Winker, M. Chiriaco, J.-L. Dufresne, and G. Sèze, 2008: Use of CALIPSO lidar observations to evaluate the cloudiness simulated by a climate model, Geophys. Res. Lett., 35, L15704, doi:10.1029/2008GL034207.

Chepfer, H., S. Bony, D. Winker, G. Cesana, J.-L. Dufresne, P. Minnis, C. J. Stubenrauch, and S. Zeng, 2010: The GCM-Oriented CALIPSO Cloud Product (CALIPSO-GOCCP), J. Geophys. Res., 115, D00H16, doi:10.1029/2009JD012251

De Haan J., P. B. Bosma, and J. W. Hovenier, 1986: The adding method for multiple scattering of polarized light, *Astron. Astrophys*., *183*, 371-391.

Deschamps, P-Y., F-M. Bréon, M. Leroy, A. Podaire, A. Brickaud, J-C. Buriez, and G. Sèze, 1994 : « The POLDER Mission : Instrument Characteristics and Scientific Objectives », *IEEE*, 32, 598-615.

Dufresne J.-L., and S. Bony, 2008: An assessment of the primary sources of spread of global warming estimates from coupled atmosphere-ocean models. J. Climate, 21(19), 5135-5144, doi: 10.1175/2008JCLI2239.1.

Dufresne J.-L. et al., 2013: Climate change projections using the IPSL-CM5 Earth System Model: from CMIP3 to CMIP5. *Clim. Dynamics*, 40(9-10), 2123-2165, doi: 10.1007/s00382-012-1636-1

Emanuel, K. A., 1991: A scheme for representing cumulus convection in large-scale models, J. Atmos. Sci., 48, 2313–2335.

Fougnie, B., G. Bracco, B. Lafrance, C. Ruffel, O. Hagolle, and C. Tinel, 2007 : PARASOL in-flight calibration and performance, Appl. Opt., 46, 5435–5451.

Grandpeix, J.-Y. and J.-P. Lafore, 2010: A density current parametrization coupled with Emanuel's convection scheme. Part I: The models, J.Atmos. Sci., 67, 881-897.

Hale G. M. and M. R. Querry, 1973: Optical constants of water in the 200nm to 200mm wavelength region, *Appl. Opt*., 12, 555-63.

Haynes, J.M., R.T. Marchand, Z. Luo, A. Bodas-Salcedo and G.L. Stephens, 2007: A Multipurpose Radar Simulation Package: QuickBeam, Bull. Amer. Met. Soc., 88, 1723-1727.

Hourdin, F., I. Mousat, S.Bony, P. Braconnot, F. Cordon, J.-L. Dufresne, L. Fairhead, M.-A. Filiberti, P. Friedlingstein, J.-Y. Grandpeix, G. Krinner, P. Le Van, Z.-X. Li and F. Lott, 2006: The LMDZ general circulation model: climate performance and sensitivity to parameterized physics with emphasis on tropical convection. *Climate Dynamics*, 19 (15), 3445-3482, DOI: 10.1007/s00382-006-0158-0.

Hourdin F., M.A. Foujols, F. Codron, V. Guemas, J.-L. Dufresne, S. Bony, S. Denvil, L. Guez, F. Lott, J. Gatthas, P. Braconnot, O. Marti, Y. Meurdesoif and L. Bopp (2013-a): From LMDZ4 to LMDZ5 : impact of the atmospheric model grid configuration on the climate and sensitivity of IPSL climate model, *Climate Dynamics*, 40(9-10), 2167-2192, doi: 10.1007/s00382-012-1411-3

Hourdin F., J.-Y. Grandpeix, C. Rio, S. Bony, A. Jam, F. Cheruy, N. Rochetin, L. Fairhead, A. Idelkadi, I. Musat, J.-L. Dufresne, M.-P. Lefebvre, A. Lahellec and R. Roehrig (2013-b): From LMDZ5A to LMDZ5B : revisiting the parameterizations of clouds and convection in the atmosperic component of the IPSL-CM5 climate model, *Climate Dynamics*, 40(9-10), 2193-2222, doi: 10.1007/s00382-012-1343-y.

Jakob, C., and G. Tselioudis, 2003: Objective identification of cloud regimes in the Tropical Western Pacific, Geophys. Res. Lett., 30(21), 2082, doi:10.1029/2003GL018367.

Jam A, F. Hourdin, C. Rio and F. Couvreux, 2011: Resolved versus parametrized boundary-layer plumes. part iii: A diagnostic boundary-layer cloud parameterization derived from large eddy simulations, B.L.M. , submitted

Kawai H and Texeira, J. 2012. Probability density functions of liquid water path and total water content of marine boundary layer clouds: implications for cloud parameterization, J. Climate, 25, 2162-2177, DOI: 10.1175/JCLI-D-11-00117.1

Klein, S.A., and C. Jacob, 1999: Validation and sensitivities of frontal clouds simulated by the ECMWF model. Mon. Weather Rev., 127, 2514-2531.

Klein, S.A.,Y. Zhang, M.D. Zelinka, R. Pincus, J. Boyle, and P. J. Gleckler (2013), Are climate model simulations of clouds improving? An evaluation using the ISCCP simulator, *J. Geophys. Res. Atmos.*, 118, 1329–1342, doi:10.1002/jgrd.50141.

Konsta, D., H. Chepfer, and J.-L. Dufresne, 2012: A process oriented representation of tropical oceanic clouds for climate model evaluation, based on a statistical analysis of daytime A-train high spatial resolution observations, Climate Dynamics, 39(9-10), 2091-2108, doi:10.1007/s00382-012-1533-7

Li J, Dobbie S, Raisanen P, Min Q. 2005. Accounting for unresolved clouds in a 1-D solar radiative transfer model. Q. J. Roy. Meteorol. Soc. 131: 1607-1629.

Liu, Z., A. Omar, M. Vaughan, J. Hair, C. Kittaka, Y. Hu, K. Powell, C. Trepte, D. Winker, C. Hostetler, R. Ferrare, and R. Pierce, 2008: CALIPSO lidar observations of the optical properties of Saharan dust: A case study of lomg-range transport, J. Geophys. Res., 113, D07207, doi:10.1029/2007JD008878.

Loeb N. G., B. A. Wielicki, D. R. Doelling, G. L. Smith, D. F. Keyes, S. Kato, N. Manalo-Smith and T. Wong, 2009: Toward Optimal Closure of the Earth's Top-of-Atmosphere Radiation Budget. J. Climate, 22(3), 748-766, doi: 10.1175/2008JCLI2637.1

Mace G. G. and F. J. Wrenn, 2013: Evaluation of the Hydrometeor Layers in the East and West Pacific within ISCCP Cloud-Top Pressure-Optical Depth Bins Using Merged CloudSat and CALIPSO Data. J. Climate, 26, 9429-9444.

Marchand R., J. Haynes, G.G. Mace, T. Ackerman, and G. Stephens, 2009: A comparison of simulated cloud radar output from the multiscale modeling framework global climate model with CloudSat cloud radar observations. J. Geophys. Res., 114, D00A20, doi:10.1029/2008JD009790.

Marti, O., P. Braconnot, J.-L. Dufresne, J. Bellier, R. Benshila, S. Bony, A. Caudel, F. Cordon, N. de Noblet, S. Denvil, L.

Fairhead, T. Fichefet, M.-A. Foujols, P. Friedlingstein, H. goosse, J.-Y. Grandpeix, E. Guilyardi, F. Hourdin, A. Idelkadi, M. Kageyama, G. Krinner, C. Levy, G. Madec, J. Mignot, I. Musat, D. Swingedow, C. Talandier, 2010: Key features of the IPSL ocean atmosphere model and its sensitivity to atmospheric resolution, Clim. Dyn., 34, 1-26.

Martins, E., V. Noel, and H. Chepfer, 2011: Properties of cirrus and subvisible cirrus from CALIOP, related to atmospheric dynamics and water vapor, J. Geophys. Res., 116, D02208.

Medeiros, B., L. Nuijens, C. Antoniazzi, and B. Stevens, 2010: Low-latitude boundary layer clouds as seen by CALIPSO, J. Geophys. Res., 115, D23207, doi:10.1029/2010JD014437

Medeiros, B., and B. Stevens, 2011: Revealing differences in GCM representations of low clouds, Clim. Dyn., 36,385-399

Minnis, P., W. L. Jr. Smith, D. P. Garber, J. K. Ayers, and D. R. Doelling, 1955: Cloud Properties Derived from GOES-7 for the Spring 1994 ARM Intensive Observing Period Using Version 1.0.0 of the ARM Satellite Data Analysis Program. NASA RP 1366, 59.

Nam, C.; Bony, S.; Dufresne, J.-L.; Chepfer, H., 2012; The "too few, too bright" tropical low-cloud problem in CMIP5 models. *Geophys. Res. Lett.*, 39(21), L21801, doi: 10.1029/2012GL053421

Noel, V., A. Hertzog, H. Chepfer, and D. M. Winker, 2008: Polar stratospheric clouds over Antarctica from the CALIOP spaceborn lidar, J. Geophys. Res., 113, D02205, doi:10.1029/2007JD008616

Noel, V. and H. Chepfer, 2010: A global view of horizontally-oriented crystals in ice clouds from CALIPSO, J. Geophys. Res., 115, D012365.

Parol F., J.C. Buriez, C. Vanbauce, J. Riedi, L. C.-Labonnote, M. Doutriaux-Boucher, M. Vesperini, G. Sèze, P. Couvert, M. Viollier, F.M. Bréon , 2004 : Capabilities of multi-angle polarization cloud measurements from satellite: POLDER results, *Adv. Space Res.* , 33, 1080-1088

Pincus R, Klein SA., 2000. Unresolved spatial variability and microphysical process rates in large-scale models. J. Geophys. Res. 105(D22): 27059-27065.

Pitts, M.C., L.W. Thomason, L.R. Poole, and D.M. Winker, 2007: Characterization of Polar Stratospheric Clouds with Space-Borne Lidar: CALIPSO and the 2006 Antarctic Season, Atmos. Chem. Phys. Discuss., 7, 7933-7985.

Randall, D. A., R. A. Wood, S. Bony, R. Colman, T. Fichefet, J. Fyfe, V. Kattsov, A. Pitman, J. Shukla, J. Srinivasan, R. J. Stouffer, A. Sumi and K. E. Taylor, 2007 : Climate Models and Their Evaluation. In: *Climate Change 2007: The Physical Science Basis. Contribution of Working Group I to the Fourth Assessment Report of the Intergovernmental Panel of Climate Change* [Solomon, S., D. Qin, M. Manning, Z. Chen, M. Marquis, K. B. Averyt, M. Tignor and H.L. Miller (eds.)]. Cambridge University Press, Cambridge, United Kingdom and New York, NY, USA.

Rio, C., J-Y Grandpeix, F. Hourdin, F. Guichard, F. Couvreux, J-P Lafore, A. Fridlind, A. Mrowiec, R. Roehrig, N.

Rochetin, M.-P. Lefebvre, A. Idelkadi (2013). Control of deep convection by sub-cloud lifting processes: the ALP closure in the LMDZ5B general circulation model; *Climate Dynamics*, 40, 2271-2292, doi:10.1007/s00382-012-1506-x

Rio, C. and F. Hourdin, 2008: A Thermal Plume Model for the Convective Boundary Layer: Representation of Cumulus Clouds, J. Atmos. Sci., 65, 407-425.

Rio, C., F. Hourdin, F. Couvreux and A. Jam, 2010: Resolved Versus Parametrized Boundary-Layer Plumes. Part II: Continuous Formulations of Mixing Rates for Mass-Flux Schemes. Boundary-layer Meteorol 135:469–483, 10.1007/s10546-010-9478-z

Rossow, W. B., and R. A. Schiffer, 1991: ISCCP cloud data products, Bull. Amer. Meteorol. Soc., 72, 2 – 20.

Rossow, W. B., G. Tselioudis, A. Polak, and C. Jakob, 2005: Tropical climate described as a distribution of weather states indicated by distinct mesoscale cloud property mixtures, Geophys. Res. Lett., 32, L21812, doi:10.1029/2005GL024584.

Sassen K., Z. Wang, and D. Liu, 2008: Global distribution of cirrus clouds from CloudSat/Cloud-Aerosol Lidar and Infrared Pathfinder Satellite Observations (CALIPSO) measurements, J. Geophys. Res., 113, D00A12, doi:10.1029/2008JD009972.

Siebesma A.P., C.S. Bretherton, A. Brown, A. Chlond, J. Cuxart, P.G. Duynkerke H. Jiang, M. Khairoutdinov, D. Lewellen, C-H. Moeng, E. Sanchez, B. Stevens and D.E. Stevens, 2003: A Large-Eddy Simulation intercomparison study of shallow cumulus convection, J.Atmos.Sci. 60 1201-1219

Simmons A., S. Uppala, D. Dee, S. Kobayashi, 2007: ERA-interim: new ECMWF reanalysis products from 1989 onwards, ECMWF Newsl., 110, 29-35

Soden B. J. and I. M. Held, 2006: An assessment of climatee feedbacks in coupled ocean-atmosphere models. J. Climate, 19, 3354-3360.

Stubenrauch C, W. Rossow, S. Kinne, 2012: Assessment of Global Cloud Data Sets from Satellites, A Project of the World Climate Research Programme Global Energy and Water Cycle Experiment (GEWEX) Radiation Panel, WCRP Report No. 23/2012

Vial, J. , J-L Dufresne, S. Bony, 2013. On the interpretation of inter-model spread in CMIP5 climate sensitivity estimates; *Clim. Dynamics*, 41, 3339-3362, doi: 10.1007/s00382-013-1725-9

Vuolo R.M., H. Chepfer, L. Menut, and G. Cesana, 2009: Comparison of mineral dust layers vertical structures modeled with CHIMERE-DUST and observed with the CALIOP lidar, *J. Geophys. Res.*, 114, D09214, doi:10.1029/2008JD011219.

Warren S. G. , 1984: Optical constants of ice from the ultraviolet to the microwave., Appl. Opt., 23, 1206-25.

Webb M., C. Senior, S. Bony and J.-J. Morcrette, 2001: Combining ERBE and ISCCP data to assess clouds in three climate models, *Climate Dynamics*, 17, 905-922.

Webb, M. J., C. A. Senior, D. M. H. Sexton, W. J. Ingram, K. D. Williams, M. A. Ringer, B. J. McAvaney, R. Colman, B. J. Soden, R. Gudgel, T. Knutson, S. Emori, T. Ogura, Y. Tsushima, N. G. Andronova, B. Li, I. Musat, S. Bony, and K. E. Taylor, 2006: On the contribution of local feedback mechanisms to the range of climate sensitivity in the two GCM ensembles. Clim. Dyn., 27, 17-38, doi: 10.1007/s00382-006-0111-2.

Williams, K. D., and G. Tselioudis, 2007: GCM intercomparison of global cloud regimes: present-day evaluation and climate change response. Clim. Dyn., 29, 231-250, doi: 10.1007/s00382-007-0232-2.

Winker D., W. Hunt, and M. McGill, 2007: Initial Performance Assessment of CALIOP, *Geophys. Res. Lett*., 34, L19803, doi:10.1029/2007GL030135.

Yang P., K. N. Liou, K. Wyser, D. Mitchell, 2000: Parameterization of the scattering and absorption properties of individual ice crystals., *J. Geophys. Res*., 105, 4699-4718.

Yang P., B-C. Gao, B. A. Baum, W. J. Wiscombe, Y. X. Hu, S. L. Nasiri, P. F. Soulen, A. J. Heymsfield, G. M., Mc Farquhar, and L. M. Miloshevich, 2001: Sensitivity of cirrus bidirectional reflectance to vertical inhomogeneity of ice crystal habits and size distributions for two Moderate-Resolution Imaging Spectroradiometer (MODIS) bands , *J. Geophys. Res*, 106, 17267-17291.

Yu W., M. Doutriaux, G. Seze, H. Le Treut, and M. Desbois, 1996: A methodology study of the validation of clouds in GCMs using ISCCP satellite observations. Clim. Dyn., 12: 389-401.

Zhang M H, W.Y. Lin, S.A. Klein, J.T. Bacmeister, S.Bony, R.T. Cederwall, A.D. Del Genio, J.J. Hack, N.G. Loeb, U. Lohmann, P. Minnis, I. Musat, R. Pincus, P. Stier, M.J. Webb, J.J.B. Wu, S.C. Xie, M.-S. Yao, and J.H. Zhang, 2005: Comparing Clouds And Their Seasonal Variations in 10 Atmospheric General Circulation Models With Satellite Measurements, *J. Geophys. Res.*, 110, D15S02, doi:10.1029/2004JD005021.

Zhang Y., S.A. Klein, J. Boyle, and G.G. Mace, 2010: Evaluation of tropical cloud and precipitation statistics of Community Atmosphere Model version 3 using CloudSat and CALIPSO data. J. Geophys. Res., 115, D12205, doi:10.1029/2009JD012006.

Annex

Annex A: Spatio-temporal sampling of CALIPSO and PARASOL observations

(i) Temporal resolution:

The two instruments follow the same sun-synchronous A-train orbit, which passes over each location twice a day at about 1:30 AM and 1:30 PM local solar time. As PARASOL collects measurements during daytime, only the daytime CALIPSO data are considered. The two instruments fly over the same orbit so they document the same cloud parcel simultaneously at about 1:30 AM local solar time.

The incomplete sampling of the diurnal cycle has negligible impact (less than 1%) on the results [Chepfer et al., 2008].

(ii) Spatial resolution

As a PARASOL pixel (6x6km) is much larger than a CALIOP/CALIPSO one (330m along-track, 75m cross-track), one value of the directional reflectance is associated to at least 18 lidar profiles. To overcome these differences, the CALIOP cloud cover and the PARASOL reflectance are processed independently on a statistical basis and then compared to daily mean values on a 2°x2° grid (several hundreds of km^2). To test the impact of the sampling over seasonal mean results on a 2°x2° grid, two PARASOL reflectance datasets were built in the same viewing direction (θ_v=27°,ϕ_s-ϕ_v=320°): the first dataset includes all reflectance values measured by PARASOL, and the second dataset includes only the reflectance measured along the CALIPSO ground track. The maximum distance between a PARASOL and a CALIOP pixel in the first dataset is 50km. The number of measurements is about 30% lower in the second dataset. Maps of 2°x2° mean directional reflectances and variances (not shown) are similar for both datasets although the second one is noisier, thus suggesting that both PARASOL datasets (collocated or not with CALIOP) can be analyzed. The similarity between the two datasets also shows that the few PARASOL pixels collocated with CALIOP (6x6 km2) are representative of all PARASOL pixels included in the 2°x2° grid cell.

Similarly, it is thus reasonable to consider that the CALIOP dataset (even with a 330mx75m resolution) when averaged over several months is statistically representative of the monthly/seasonal cloud cover within a GCM grid cell.

Annex B: Sensitivity of the PARASOL monodirectional reflectance to the atmosphere's composition

(i) Optical properties

The cloud particle optical properties (e.g. single scattering albedo, scattering phase function, extinction coefficient) depend on the wavelength, the particle size and its shape. As the absorption phenomena is negligible in both ice and water at 864nm [Warren et al 1984 ; Hale and Querry, 1973], the single scattering albedo is close to one regardless of the size and shape of the particles. As the radius of cloud particles are always larger than the wavelength considered here, the scattering phase function is not very sensitive to the droplet size but it is sensitive to the particle shape. A spherical shape assumption, which is typical of liquid water computed with the Mie theory and a non-spherical shape, which is typical [Chepfer et al. 2002] of ice crystals whose optical properties are computed with Geometric Optic enhanced with Finite Differential Time Domain [Yang et al 2000 and 2001] are used. As shown in Fig. C.a, their scattering phase functions differ significantly for scattering angles close to backscattering (180°), haloes (22° and 44°) and rainbow (140°), and also between 90° and 130°, which corresponds to the viewing and solar zenith angle selected for PARASOL data in the Tropics. Complementary computations (not shown) indicate that the scattering phase function (at this wavelength) weakly depends on the particle size compared to the influence of the shape. On the contrary, the particle extinction coefficient is directly dependent on the particle size: it is proportional to the scattering efficiency (close to 2 as the particles are large than the wavelength) multiplied by the particle cross section, which is expressed as the function of the particle size.

(ii) Radiative transfer computations

The directional reflectance is computed using a doubling-adding radiative transfer code [DeHaan et al. 1986]. The cloud particles optical properties such as the single scattering albedo and the truncated scattering phase function developed in Legender polynomial are introduced in the radiative transfer code. The Rayleigh scattering is also taken into account in the computation even though its contribution to the total directional reflectance remains small (τ is about 0.013 for the whole atmospheric column). As the studied viewing direction is off-glitter, the ocean is described as a lambertian surface with a constant plane albedo of 0.03. The directional reflectance is then computed as in Chepfer et al. [2002] for various cloud optical depths and solar zenith angles.

Figure C.b shows that changes of reflectance values due to solar zenith angle variations are less than 0.1 in the tropical regions (30°S-30°N, $18° < \theta_s < 60°$) for a given phase function. It reaches a maximum of 0.15 between the ITCZ and the higher observable latitudes (θ_s>60°). Thus variations of the latitudinal reflectance larger than 0.15 (0.1 in the Tropics) cannot be attributed to variations of θ_s. They are due to changes in the atmosphere composition (clouds). The sensitivity of the reflectance to the cloud particles scattering phase function is maximum at high latitudes / high solar zenith angle (0.13) and slightly reduces in the tropics (0.1).

(iii) PARASOL simulator

The PARASOL simulator is initiated with the mixing ratios of in-cloud liquid and ice water content in each model grid cell that are then converted into sub-grid mixing ratios using SCOPS. In each subcolumn, the total cloud optical depth (τ_tot) is the sum of the subcolumn ice (τ_tot_ice) and liquid (τ_tot_liq). These are computed assuming that the cloud particles are spherical with a radius equal to the effective radius predicted by the model. For five solar zenith angles (θ_s=0°, 20°, 40°, 60° and 80°) and knowing the total cloud optical depth, two directional reflectance values are then computed for each day and for each solar zenith angle assuming that the cloud is entirely composed of liquid water (Refl_liq) or ice water (Refl_ice). These reflectance values are derived from a bilinear interpolation over pre-calculated look-up tables containing results of radiative transfer computations (Annex B) for the cloud particle's shape assumption (spherical and non spherical) made in the model. The subgrid directional reflectance is then computed as follow: Refl= (Refl_liq*τ_tot_liq + Refl_ice*τ _tot_ice) / τ _tot. The directional reflectance obtained for each subgrid is then averaged over each GCM grid cell for each day and for each θ_s. After the simulations have been performed, the five monodirectional reflectances corresponding to the five solar zenith angles from the simulator's outputs are used to interpolate linearly the monodirectional reflectance depending on the monthly mean value of the solar zenith angle at each grid point. The simulated monodirectional reflectance is then directly comparable to the observations.

Figure B:

a) Scattering phase function for spherical and non-spherical particles. Monodirectional reflectance simulated as a function of the solar zenith angle for spherical and non-spherical particles in the viewing direction (θ_v = 27° ϕ_v=320°).

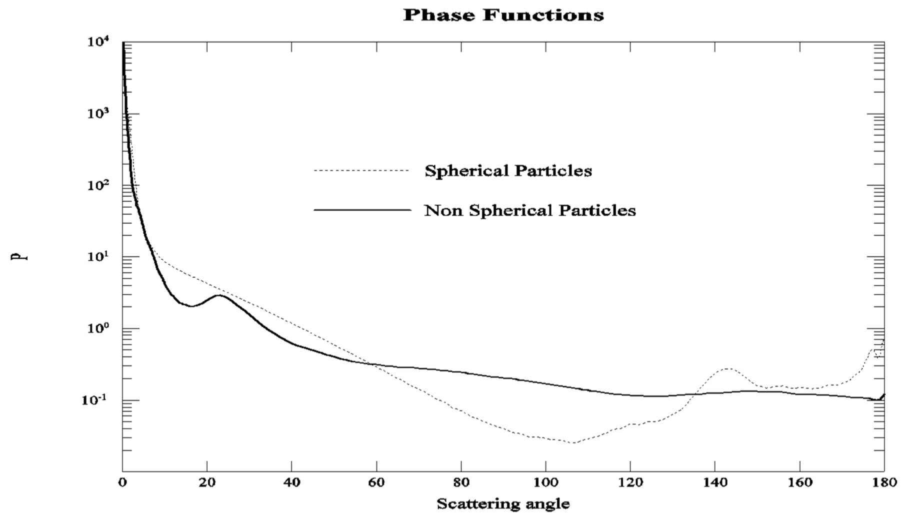
Phase Functions
Spherical Particles
Non Spherical Particles
P
Scattering angle

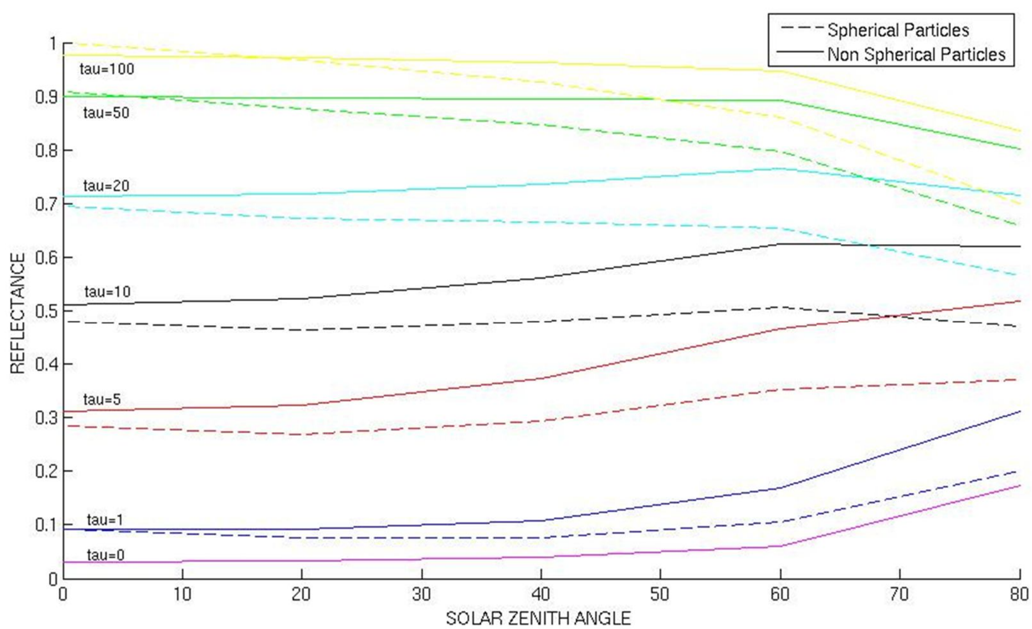
Spherical Particles
Non Spherical Particles
tau=100
tau=50
tau=20
tau=10
tau=5
tau=1
tau=0
REFLECTANCE
SOLAR ZENITH ANGLE

Annex C: Traditional global monthly mean evaluation of cloud properties

a) Cloud cover

On average, cloud cover is underestimated over the tropical regions and is broadly consistent with observations in the mid and high latitudes (Fig. C1). In the Tropical Western Pacific, along the ITCZ and the SPCZ, the cloud cover simulated by LMDZ5A is about 60-70% whereas observations indicate a cloud cover ranging from 80% to 100%. In regions where the cloud cover is low, such as in the trade wind cumulus region, observations indicate a cloud fraction between 40 and 60% whereas the simulated cloud cover is only about 20 to 50%. Although LMDZ5B underestimates the averaged cloud cover in the tropics, the bias is reduced by a factor close to 2 compared to LMDZ5A. The improvement is very significant in almost all fully overcast regions (e.g. warm-pool, east Pacific and Atlantic) and even with an overestimated cloud cover.

Figure C1 : Geographical distribution of the total mean cloud cover over the ocean averaged over the period 2007-2008 (a) observed with CALIPSO-GOCCP during day time, (b) simulated with LMDZ5A and the lidar simulator, (c) simulated with LMDZ5B and the lidar simulator; (d) zonal mean of the same quantity observed (red line) and simulated (LMDZ5A: black line and LMDZ5B: black dotted line).

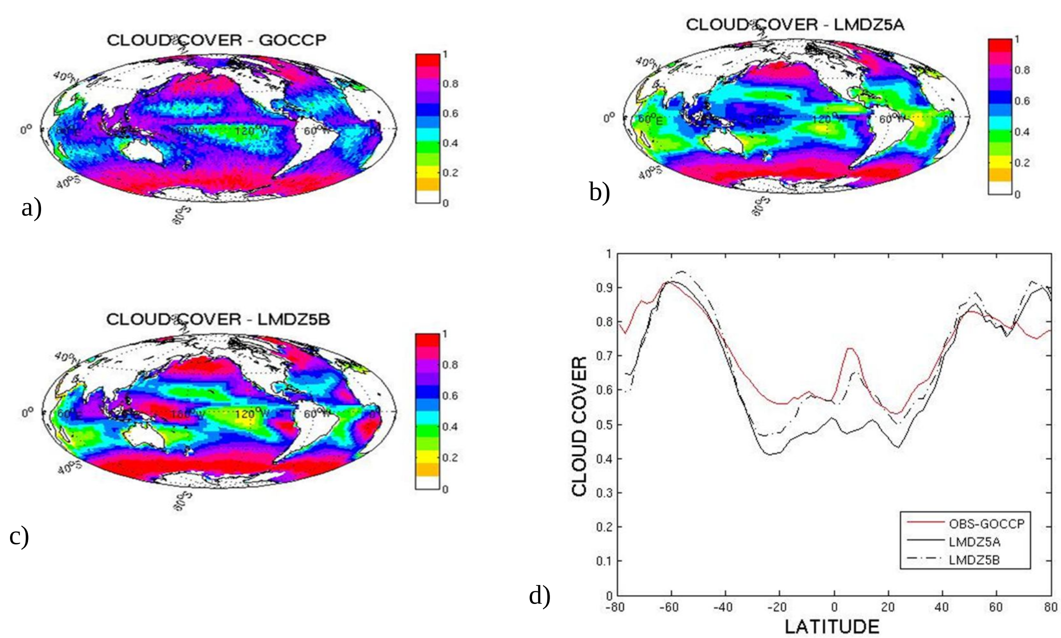

b) Cloud vertical profile

The zonal mean vertical distribution of the observed CALIPSO-GOCCP cloud fraction clearly highlights the well-known links between cloud characteristics and large circulation of the atmosphere (Fig. C2-a). The altitude of the higher clouds follows the tropopause height and decreases from the equator to the poles. The LMDZ5A model with the lidar simulator produces a cloud fraction of high-level clouds that is too large almost everywhere and the altitude of these clouds is too high, in particular over the polar region in the southern hemisphere (Fig. C2-b). In the tropics, LMDZ5A strongly underestimates the cloud fraction at low and middle altitudes. Although this feature is amplified by the masking effect of high clouds on the lidar signal (thick high level clouds, with typical Cτ>3, attenuate the signal and mask low- and mid-level clouds that might exist below them), this underestimation already occurs with the cloud cover simulated by the model (i.e. without using the lidar simulator, cf Chepfer et al., 2008). At higher latitudes, the model cannot simulate the large vertical extent of the frontal clouds associated with storms. Instead, it simulates two separate groups of low- and high-level clouds. This zonal mean vertical distribution of clouds is improved in LMDZ5B (Fig. C2-c). In the tropics, boundary level clouds are present although they are too low and too concentrated in one single layer. At middle and high latitudes, the model almost simulates the continuous vertical structure of the cloud fraction.

Figure C2: Zonal mean cloud fraction profile averaged over the period 2007-2008, a) observed from CALIPSO-GOCCP, b) simulated with LMDZ5A and the lidar simulator and c) simulated with LMDZ5B and the lidar simulator.

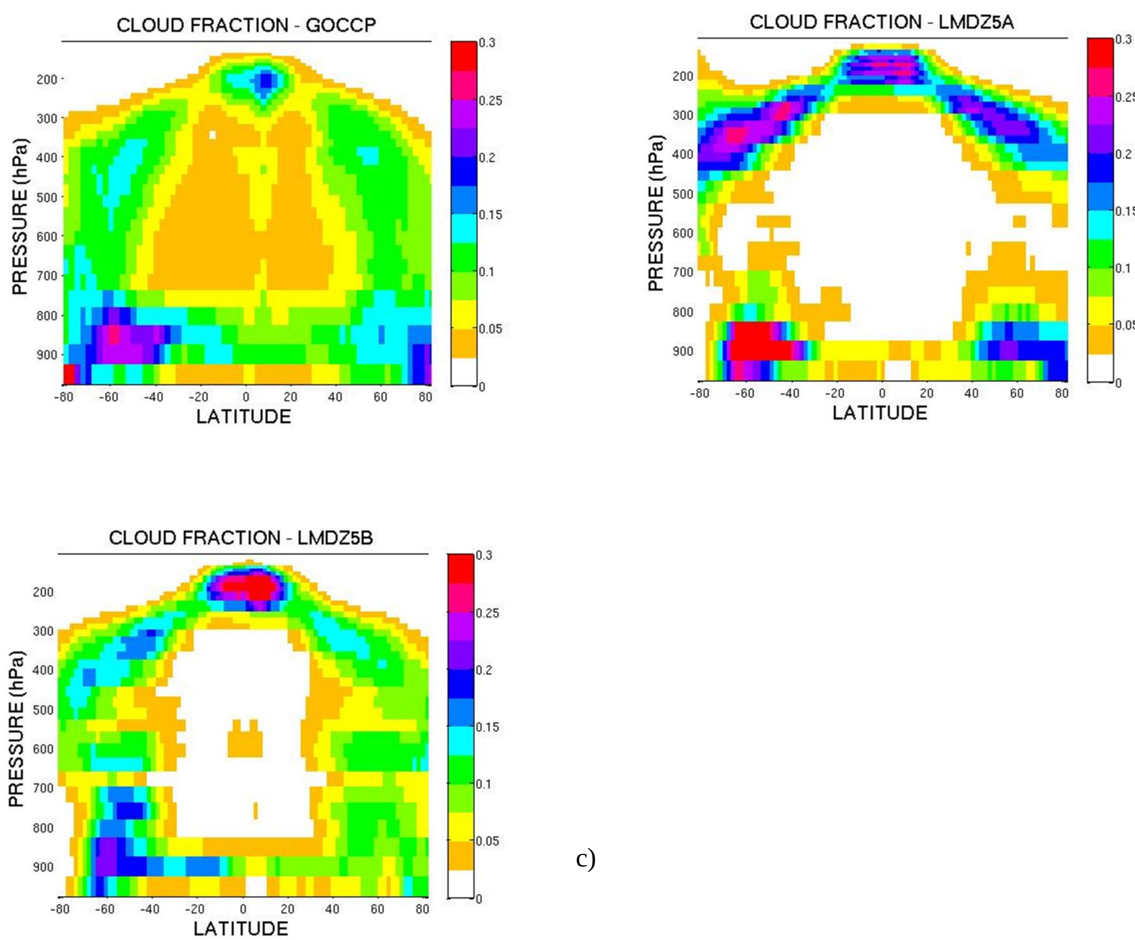

a) b)

c)

c) Cloud reflectance

In the trade wind regions, the observed cloud reflectance (typical value of 0.15) is only slightly higher than the clear-sky value (approximately 0.03), indicating that clouds are optically thin. This is not the case for the two model versions (Figure C3-b,c). They strongly overestimate the cloud reflectance almost everywhere, in particular over the subtropical oceans and in the mid and high latitudes. The models cannot reproduce the contrast between the higher values (≈0.3) of cloud reflectance observed along the ITCZ and the Eastern Pacific ocean and the lower values (<0.2) over the tropical trade wind cumulus region. They simulate high cloud reflectances (>0.2) over the tropics. On average, the cloud reflectance, and therefore the cloud optical thickness, simulated by the models over the ocean is too high almost everywhere.

Figure C3: Same as Fig. C1 for the monodirectional cloud reflectance over ocean, on average for the period 2007-2008 (a) observed with PARASOL, (b) simulated with LMDZ5A and the PARASOL simulator, (c) simulated with LMDZ5B and the PARASOL simulator; (d) zonal mean of the same quantity observed (red line) and simulated (LMDZ5A: black line and LMDZ5B: black dotted line).

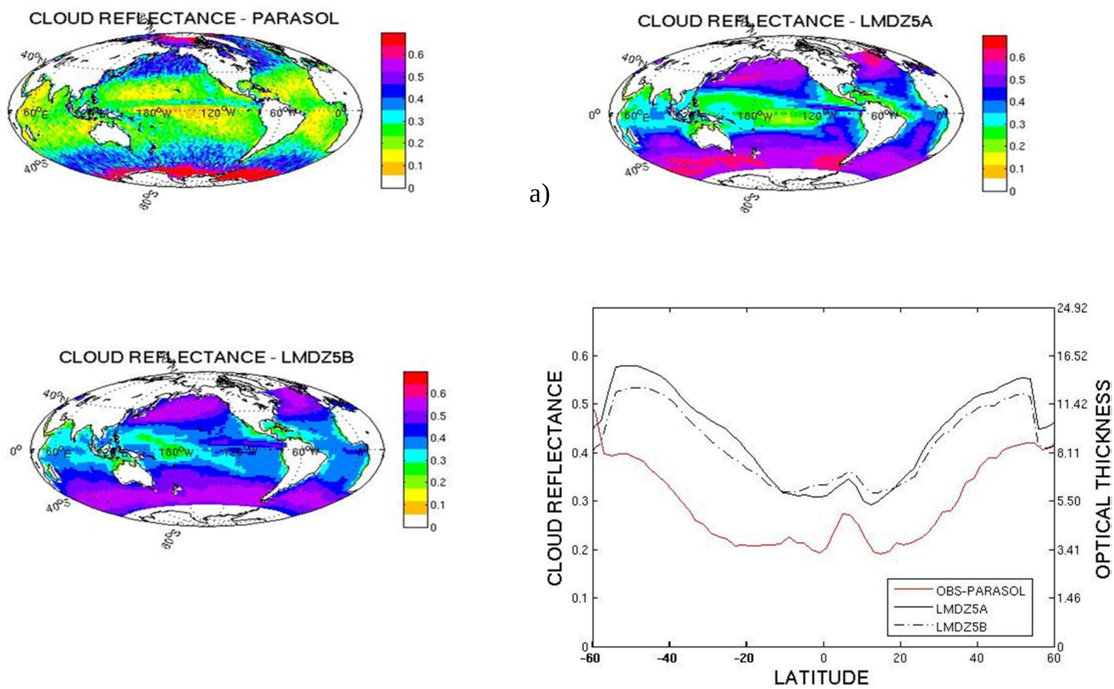

a) b) c) d)

List of Figures

1. (a) Cloud cover, (b) cloud reflectance (approximative optical depth on the right y-axis, see Sect. 2.3), (c) SW

albedo as a function of the vertical velocity ω_{500} and d) PDF of ω_{500} , observed (coloured lines), simulated with LMDZ5A (black line), simulated with LMDZ5B (black dotted line). For the cloud cover and the cloud reflectance the simulator is used for model results. All the data are monthly means over the tropical oceans. The monthly mean vertical velocity are from the ERA interim reanalysis [Simmons et al. 2007] and the short wave planetary albedo is estimated from CERES - EBAF (Clouds and the Earth's Radiant Energy System) [Loeb et al. 2009].

2. Cloud top pressure versus optical thickness (PC-tau) histograms, computed over the tropical oceans (a,d) observed, (b,e) simulated with the LMDZ5A model and the simulator and (c,f) simulated with the LMDZ5B model and the simulator. The upper line (a,b,c) corresponds to CALIPSO-GOCCP and PARASOL data (2007-2008) and simulator and the lower line (d,e,f) corresponds to ISCCP-D2 data (1983-2007) and simulator respectively. The color bar represents the number of points at each grid cell (PC-tau) divided by the total number of points in the histogram.

3. 2D histograms of cloud reflectance and cloud cover over the tropical oceans (a,d) observed with PARASOL and CALIPSO GOCCP, (b,e) simulated with LMDZ5A and the simulator, and (c,f) simulated with LMDZ5B and the simulator. The upper line (a,b,c) corresponds to instantaneous values and the lower line (d,e,f) corresponds to monthly mean values. The color bar represents the number of points at each grid cell (cloud cover-cloud reflectance) divided by the total number of points.

4. (a) PDF of cloud reflectances and (b,c,d) vertical profile of the cloud fraction CF3D for three classes defined by the grid average cloud reflectance (b) CR<0.2, (c) 0.2<CR<0.5, (d) CR>0.5. Red line corresponds to observed values from PARASOL and CALIPSO-GOCCP respectively, black line corresponds to simulated values with LMDZ5A and the simulator and black dotted line corresponds to simulated values with LMDZ5B and the simulator. The data are instantaneous values and are taken only over the tropical oceans.

5. Cumulated distribution function of the cloud cover for high level clouds (upper row) and average relationship between total cloud cover and the normalized cloud cover of high level cloud (lower row, see text) in ascent (left column) and subsidence (right column) regions, observed with CALIPSO-GOCCP (red line), simulated with LMDZ5A and the simulator (black line), and simulated with LMDZ5B and the simulator (black dotted line). The cloud cover are instantaneous values and the ascent and the subsidence regions are defined as regions over the tropical ocean where the monthly mean value of ω_{500} is respectively negative and positive.

6. 2D histograms of instantaneous cloud reflectance and cloud cover over the tropical ocean for situations where low level clouds dominate (CClow>0.9*CC) (a, d) observed, (b, e) simulated with LMDZ5A and the simulator, and (c, f) simulated with LMDZ5B and the simulator. The upper line (a,b,c) corresponds to PARASOL observations, CALIPSO

observations and simulator respectively and the lower line (d,e,f) corresponds to ISCCP. The color bar represents the number of points at each grid cell (cloud cover-cloud reflectance) divided by the total number of points.

7. Instantaneous mean cloud reflectance as a function of cloud top pressure for mainly low-cloud situations (using the criterion: CClow>0.9*CC) over the tropical ocean, observed with PARASOL and CALIPSO-GOCCP (red line), simulated with LMDZ5A and the simulator (black line), and simulated with LMDZ5B and the simulator (black dotted line).

CTP is defined as the highest level of low clouds where the local cloud cover is greater than 0.1.

8. 2D histograms of instantaneous of (**a**) cloud liquid water path versus cloud reflectance simulated with LMDZ5A for conditions where low-level-clouds dominate (CClow>0.9*CC) (**b**) cloud reflectance versus cloud cover with the modified parameterization in LMDZ5A (see text) for all clouds and (**c**) for conditions where low-level-clouds dominate (CClow>0.9*CC). The color bar represents the number of points at each grid cell divided by the total number of points.

Figures

Figure 1: (a) Cloud cover, (b) cloud reflectance (approximative optical depth on the right y-axis, see Sect. 2.3), (c) SW albedo as a function of the vertical velocity ω_{500} and d) PDF of ω_{500}, observed (coloured lines), simulated with LMDZ5A (black line), simulated with LMDZ5B (black dotted line). For the cloud cover and the cloud reflectance the simulator is used for model results. All the data are monthly means over the tropical oceans. The monthly mean vertical velocity are from the ERA interim reanalysis [Simmons et al. 2007] and the short wave planetary albedo is estimated from CERES - EBAF (Clouds and the Earth's Radiant Energy System) [Loeb et al. 2009].

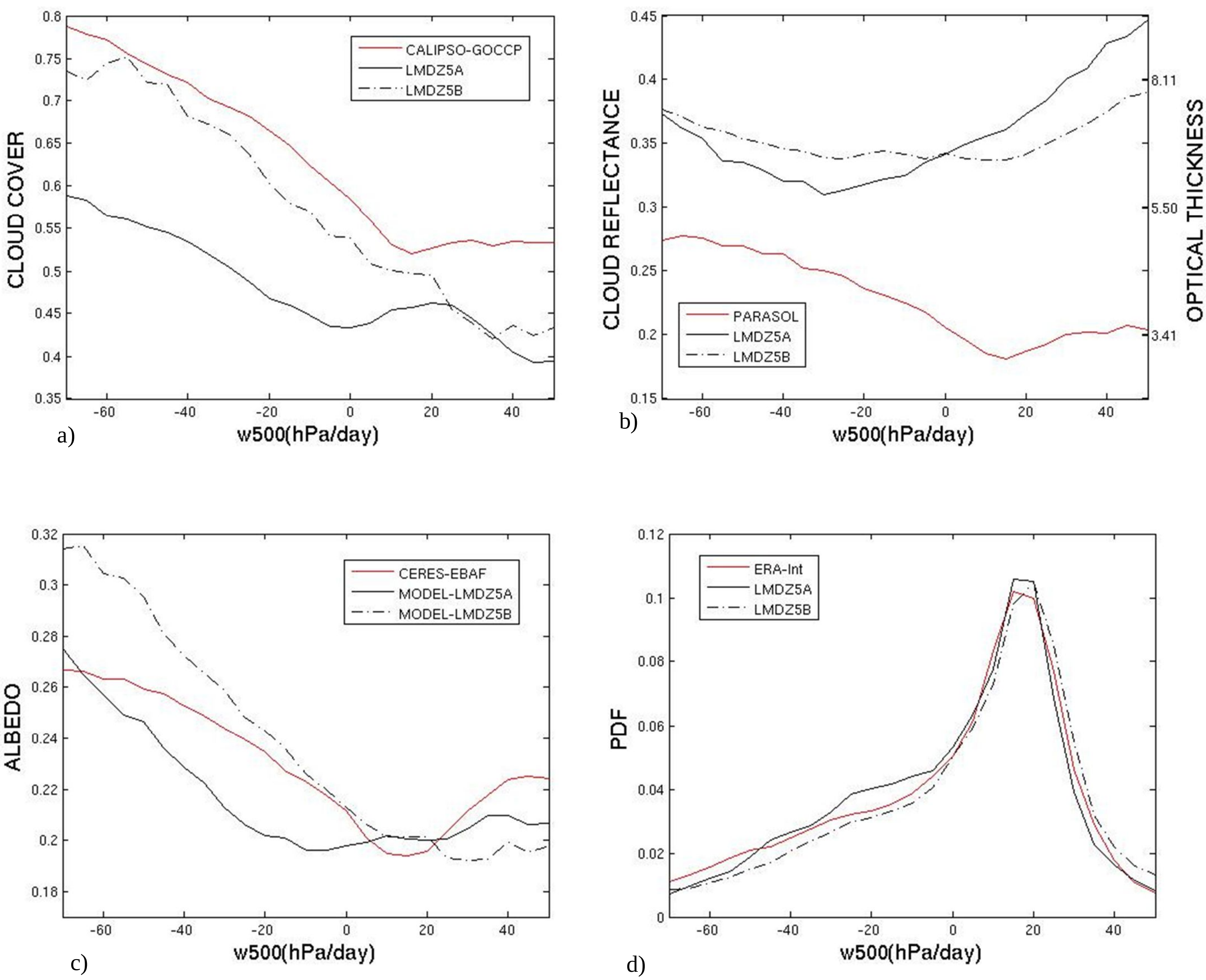

Figure 2: Cloud top pressure versus optical thickness (PC-tau) histograms, computed over the tropical oceans (a,d) observed, (b,e) simulated with the LMDZ5A model and the simulator and (c,f) simulated with the LMDZ5B model and the simulator. The upper line (a,b,c) corresponds to CALIPSO-GOCCP and PARASOL data (2007-2008) and simulator and the lower line (d,e,f) corresponds to ISCCP-D2 data (1983-2007) and simulator respectively. The color bar represents the number of points at each grid cell (PC-tau) divided by the total number of points in the histogram.

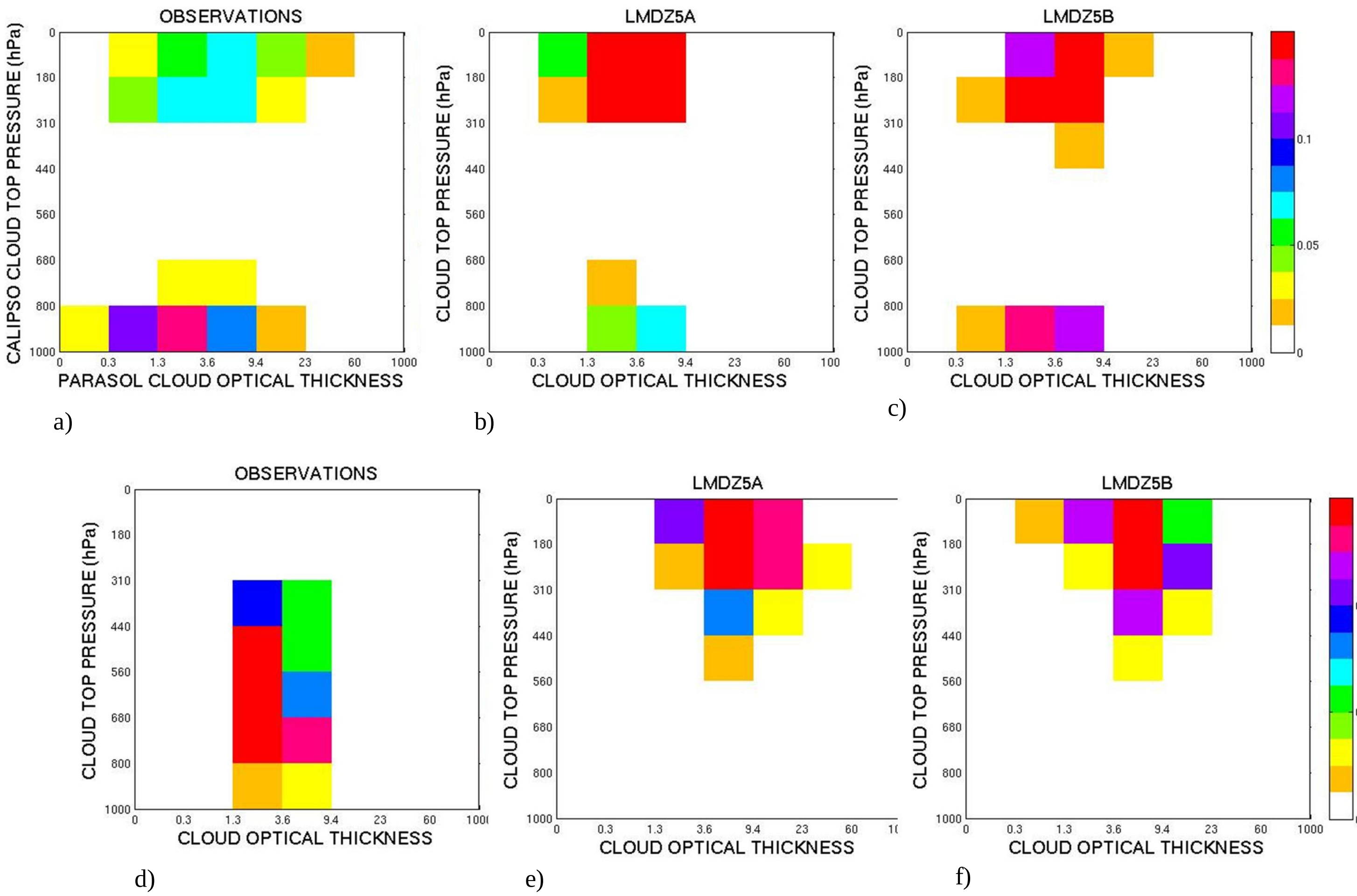

Figure 3: 2D histograms of cloud reflectance and cloud cover over the tropical oceans (a,d) observed with PARASOL and CALIPSO GOCCP, (b,e) simulated with LMDZ5A and the simulator, and (c,f) simulated with LMDZ5B and the simulator. The upper line (a,b,c) corresponds to instantaneous values and the lower line (d,e,f) corresponds to monthly mean values. The color bar represents the number of points at each grid cell (cloud cover-cloud reflectance) divided by the total number

of points.

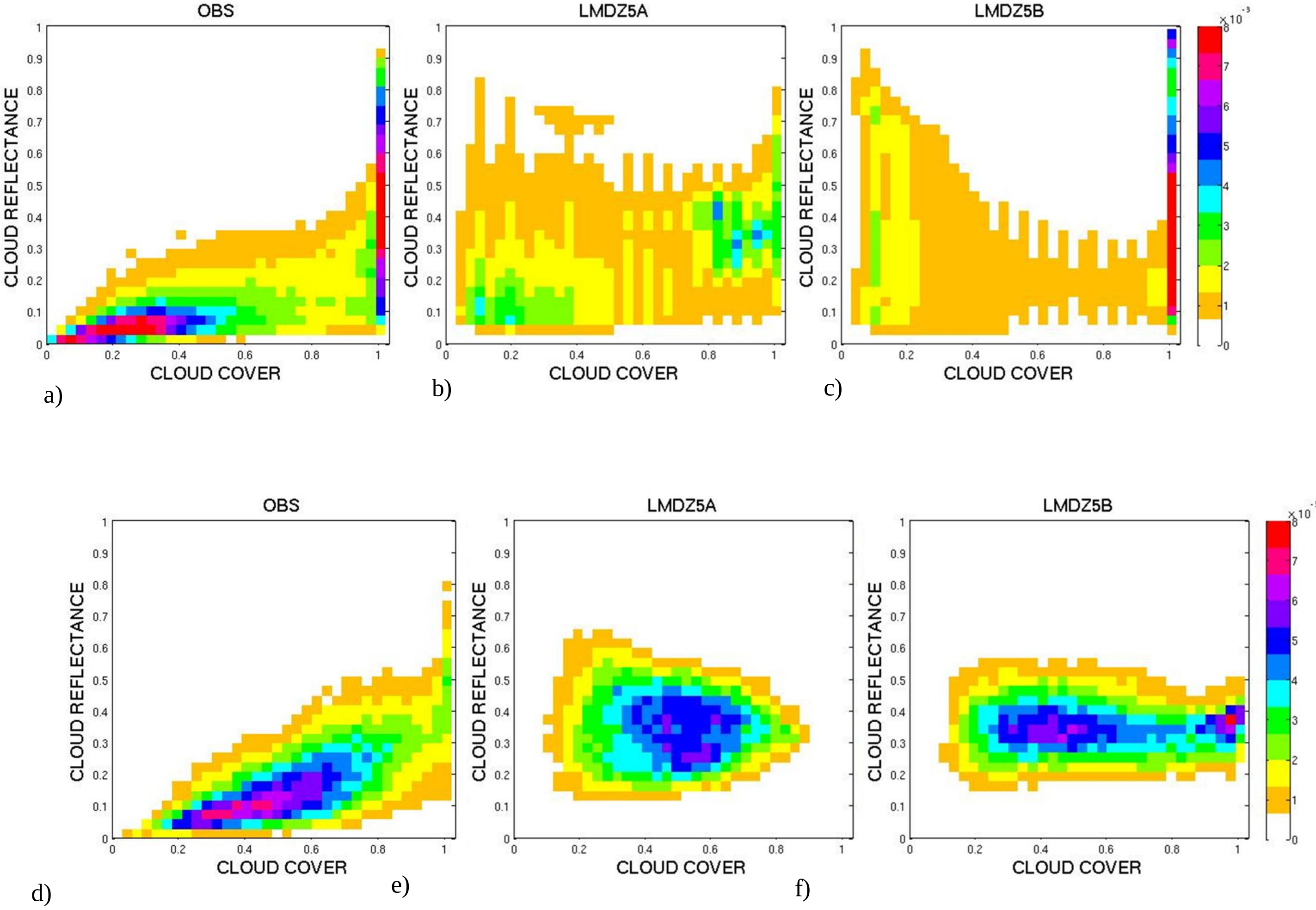

Figure 4: (a) PDF of cloud reflectances and (b,c,d) vertical profile of the cloud fraction CF3D for three classes defined by the grid average cloud reflectance (b) CR<0.2, (c) 0.2<CR<0.5, (d) CR>0.5. Red line corresponds to observed values from PARASOL and CALIPSO-GOCCP respectively, black line corresponds to simulated values with LMDZ5A and the simulator and black dotted line corresponds to simulated values with LMDZ5B and the simulator. The data are instantaneous values and are taken only over the tropical oceans.

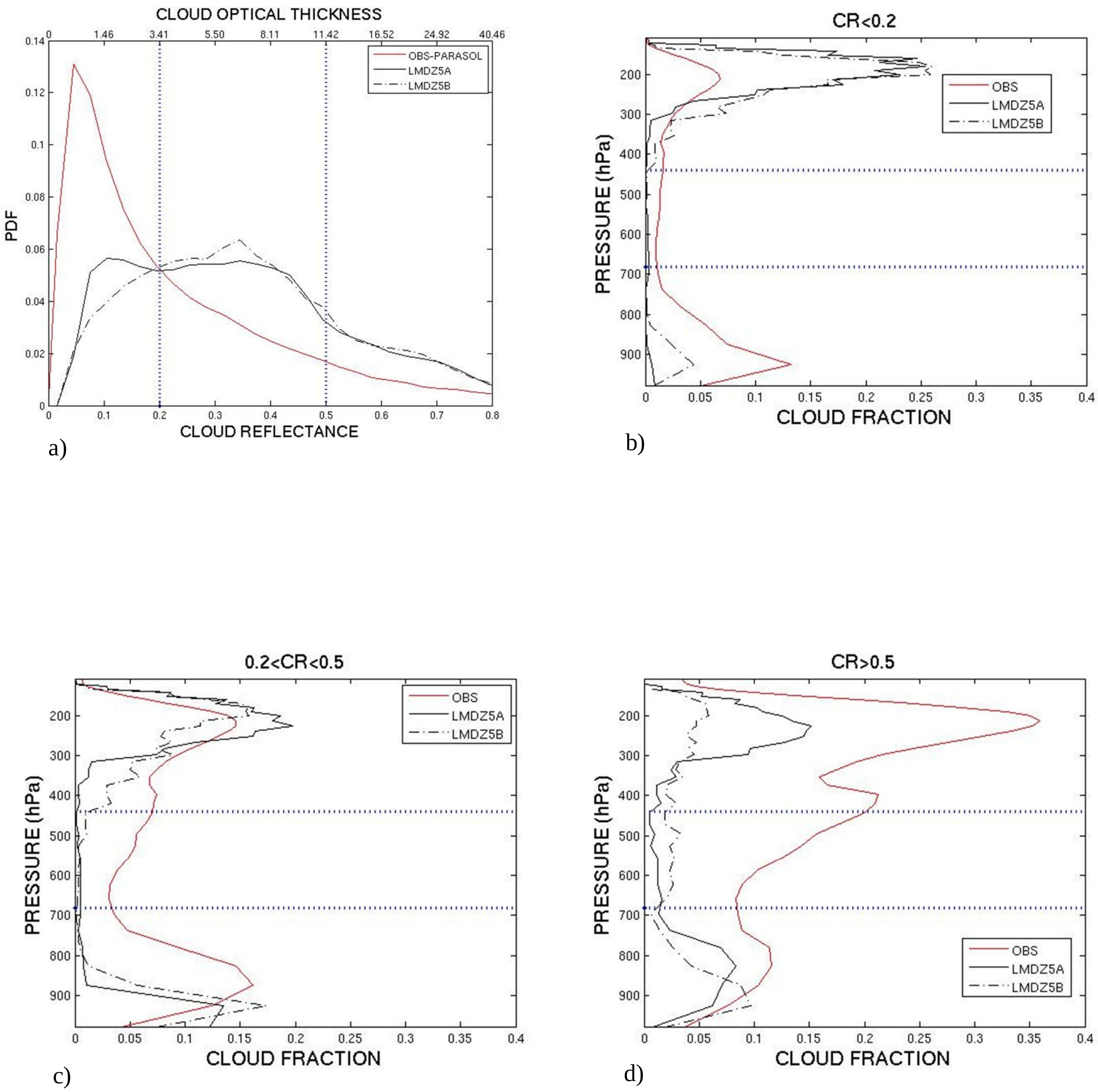

Figure 5: Cumulated distribution function of the cloud cover for high level clouds (upper row) and average relationship between total cloud cover and the normalized cloud cover of high level cloud (lower row, see text) in ascent (left column) and subsidence (right column) regions, observed with CALIPSO-GOCCP (red line), simulated with LMDZ5A and the simulator (black line), and simulated with LMDZ5B and the simulator (black dotted line). The cloud cover are instantaneous values and the ascent and subsidence regions are defined as regions over the tropical ocean where the monthly mean value of ω_{500} is respectively negative and positive.

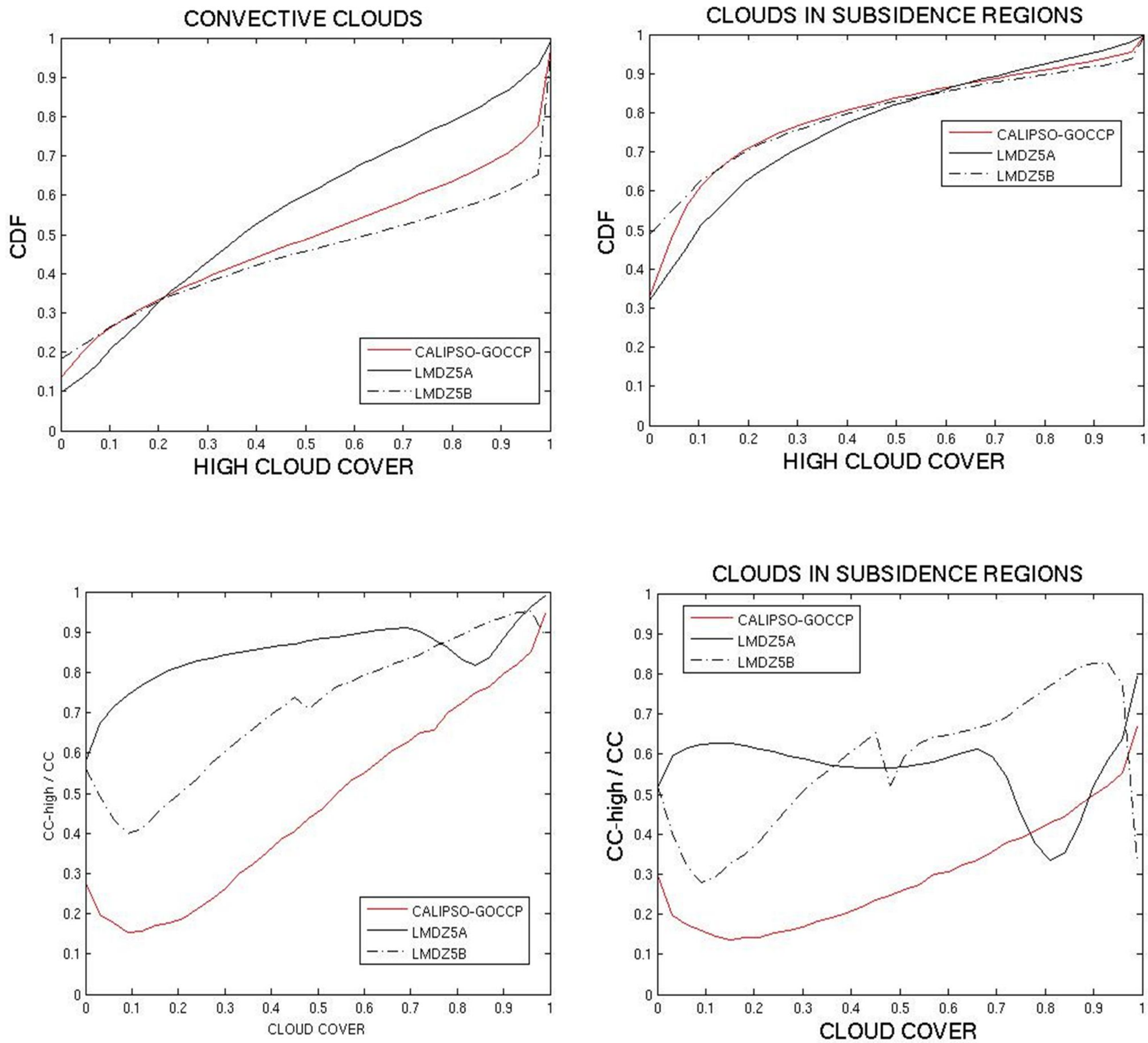

Figure 6: 2D histograms of instantaneous cloud reflectance and cloud cover over the tropical ocean for situations where low level clouds dominate (CClow>0.9*CC) (a, d) observed, (b, e) simulated with LMDZ5A and the simulator, and (c, f) simulated with LMDZ5B and the simulator. The upper line (a,b,c) corresponds to PARASOL observations, CALIPSO observations and simulator respectively and the lower line (d,e,f) corresponds to ISCCP. The color bar represents the number of points at each grid cell (cloud cover-cloud reflectance) divided by the total number of points.

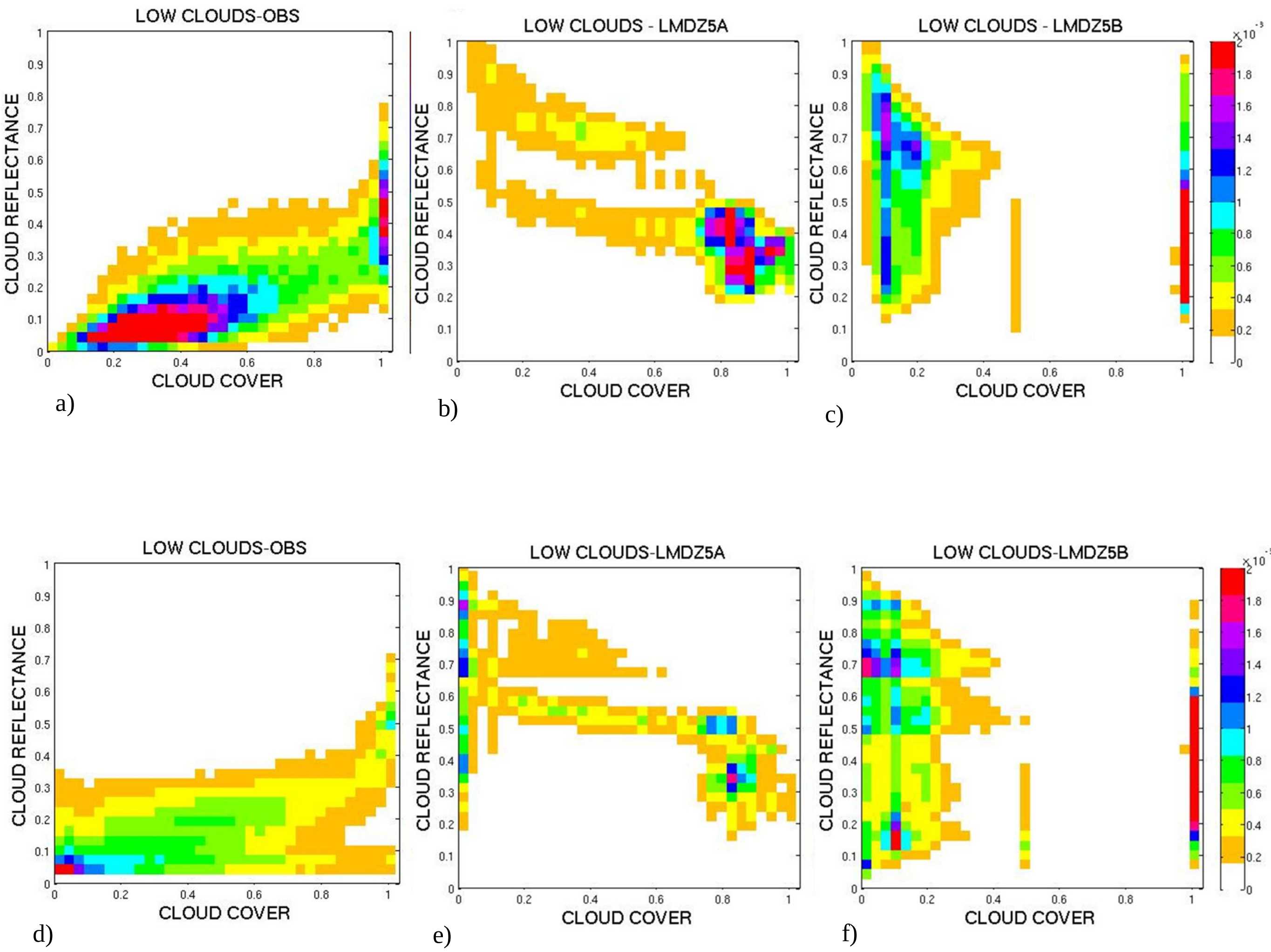

Figure 7: Instantaneous mean cloud reflectance as a function of cloud top pressure for mainly low-clouds situations (using the criterion: CClow>0.9*CC) over the tropical ocean, observed with PARASOL and CALIPSO-GOCCP (red line), simulated with LMDZ5A and the simulator (black line), and simulated with LMDZ5B and the simulator (black dotted line).

CTP is defined as the highest level of low clouds where the local cloud cover is greater than 0.1.

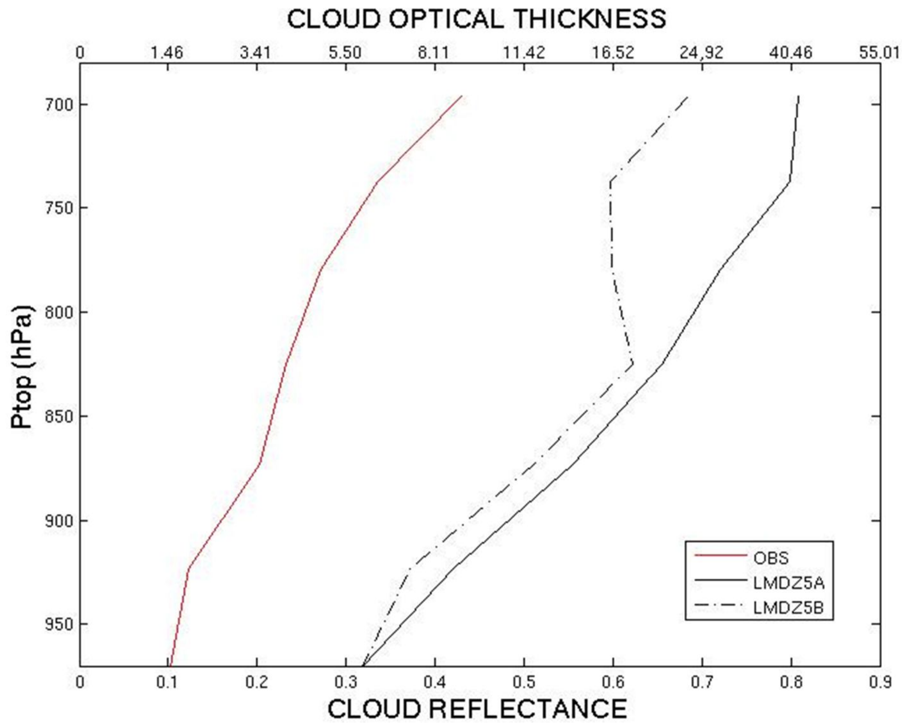

Figure 8: 2D histograms of instantaneous of (**a**) cloud liquid water path versus cloud reflectance simulated with LMDZ5A for conditions where low-level-clouds dominate (CClow>0.9*CC) (**b**) cloud reflectance versus cloud cover with the modified parameterization in LMDZ5A (see text) for all clouds and (**c**) for conditions where low-level-clouds dominate

(CClow>0.9*CC). The color bar represents the number of points at each grid cell divided by the total number of points.